



MASTER THESIS

Development of an origami based, magnetically actuated, endovascular locomotion device

JOANNES CORNELIUS SCHAGEN

FACULTY OF ENGINEERING TECHNOLOGY

DEPARTMENT OF BIOMECHANICAL ENGINEERING

EXAMINATION COMMITTEE

PROF. DR. S MISRA

DR. V. KALPATHY VENKITESWARAN

IR. E.E.G. HEKMAN

MAY 8, 2025

Thesis submitted by
Joannes Cornelius Schagen
under the supervision of
prof. dr. S. Misra,
dr. V. Kalpathy Venkiteswaran, and
ir. E.E.G. Hekman
in order to fulfil the necessary requirements to obtain a Master's degree in
Biomechanical Engineering at the University of Twente
and defended on
Friday, 8th of May, 2025

Acknowledgement

I dedicate this thesis in memory of my father, who I still hope to make proud in everything that I do.

Jan Schagen
May 8, 2025

1 Abstract

Despite the benefits of Minimally Invasive Surgery (MIS) over open surgery, MIS is not omnipresent due to multiple technical challenges. These difficulties largely stem from the learning curve required to operate the surgical tools necessary for minimally invasive surgery (MIS). It is thus not surprising that easier methods of MIS are being developed, such as capsule robots that navigate through the human body by using the peristaltic movement of the digestive tract or magnetic actuation. Applying this technology to the arteries, however, is more difficult. The smaller scale and vulnerability of the artery wall require an alternative design. This thesis aims to develop an origami-based and magnetically actuated device that could assist endovascular MIS. The MIS selected was the endovascular repair (EVAR) of Abdominal Aortic Aneurysms (AAA), from which requirements were drawn. Based on these requirements, three concepts were developed, which, after evaluation, resulted in a final concept utilizing three modules to move through an artery like a piston. The concept was then further defined, and additional requirements were set up for each module. Based on the requirements, the waterbomb tessellation and the collapsable tower were integrated into the final design. A prototype of each separate module was developed to gain insight into the behaviour of the module, and a prototype of the entire system was created. The prototypes were made by glueing PLA panels and neodymium magnets to paper with perforation lines that followed the required crease pattern's folding lines. The total system prototype provides promising evidence as a valid proof of principle, as it can locomote through a tube at a speed of up to 8.3 mm/s and expand radially by up to 30%. However, due to scale and the use of specific materials, the design is not yet realistic for endovascular applications. The prototype also cannot move backwards, but this limitation can potentially be addressed by incorporating shape memory polymers.

Table of Contents

Acknowledgement	i
1 Abstract	ii
Table of Contents	iii
List of Figures	v
List of Tables	vii
2 Introduction	1
3 Literature research	2
3.1 Design process	2
3.2 Origami engineering	2
3.3 Origami tessellations	3
3.4 Magnetic actuation	4
3.5 Living hinges	6
3.6 AAA	6
3.7 State of the art	7
3.8 Additive Manufacturing	7
4 Preliminary Design	9
4.1 Requirements	9
4.2 Ideation	10
4.3 Concepts	10
4.3.1 Self-propelled vine robot	10
4.3.2 Popping screwthread	11
4.3.3 Negative-poison ratio worm	12
4.4 Choosing a concept to continue	12
4.5 Conclusion of preliminary design	13
5 Final design	14
5.1 Locomotion	14
5.2 Additional Requirements	16
5.2.1 Requirements for RM	16
5.2.2 Requirements for AXM	17
5.3 Origami patterns	17
5.3.1 Origami pattern for RM	17
5.3.2 Origami pattern for AXM	20
5.4 Fabrication method	22
5.4.1 3D printing	22
5.4.2 Mould with resin	22
5.4.3 Mould with sheet	22
5.5 Magnet placement	24
5.5.1 Magnet placement for RM-module	24
5.5.2 Magnet placement for AXM-module	27
5.6 Integration	28
5.7 Conclusion of final design	28

6	Module experiments	30
6.1	Setup	30
6.2	Quasi-static input	30
6.3	Square wave input	33
6.4	Conclusion of module experiments	33
7	Integration experiment	35
7.1	Setup	35
7.2	Results of integration experiments	36
7.3	Optimising phase duration	38
7.4	Phase analysis	38
7.5	Backwards motion	39
7.6	Conclusion of integration experiment	40
8	Evaluation and discussion	41
8.1	Requirements met	41
8.2	Requirements not met	42
8.3	Requirements that need to be tested	42
8.4	Conclusion of evaluation	43
9	Future research	44
9.1	Solving unmet requirements	44
9.2	Future design	44
9.3	Potential uses	45
10	Conclusion	46
	References	47
11	Appendix	52
11.1	Morphological diagram	52
11.2	Lasercutter setup	53
11.3	Lasercutter results	54
11.3.1	Results 50g paper	54
11.3.2	Results 80g paper	55
11.3.3	Result table	56
11.4	Mass-spring-damper model	57
11.4.1	background	57
11.5	Mass-spring-damper model	57
11.5.1	MSD	57
11.5.2	Creating the model	58
11.5.3	Finding the correct parameters	59
11.5.4	Using the model to find prototype improvements	60
11.5.5	Shortcomings of the model	60
11.5.6	Conclusion	61
11.6	Results integration experiment	62

List of Figures

1	(a) and (b): pictures of origami crane flapping its wings [7]. c: crease pattern of an origami crane, with mountain and valley folds [8]	3
2	Picture showing how origami engineering is used in satellites and how their crease pattern can be recreated with paper. [3]	3
3	Example of a 3x4 tessellating crease pattern	4
4	Tessellation patterns of interest for this thesis (a)Waterbomb, (b)Lang Oval Tessellation, (c)Hoffman waterbomb, (d)Hoffman star-triangles,(e)Resch triangle tessellation. [10]	4
5	Diagram showing the forces created by the bipolar magnet inside a uniform magnetic field resulting in the rotation of the magnet.	5
6	Sketch of how magnets can be used to move origami, with a) being the initial state of the origami. b) showing the forces acting on the initial state of the origami once a magnetic field is applied and c) the resulting end state of origami pattern.	5
7	Living hinges as used in the Robotime electric guitar [11]	6
8	Venn Diagram visualising the current state of the art of magnetically actuated, origami-based, endovascular devices. A: Magnetically actuated, origami-inspired endoscope capsule. B: Origami-based ICMRI catheter. C: Compliant magnetic capsule robot to traverse the aorta. [30] [59] [61]	7
9	Step-by-step visualisation of the working of the koleidocycle, starting with (a), then (b), until (e). After (e) the cycle starts again with (a). [26]	11
10	Sketch of the self-propelled vine robot pulling a stent	11
11	Sketch of the popping screwthread concept	12
12	Early concept sketch of the Negative-poison ratio worm, consisting of 6 identical modules. . .	12
13	Sketch of the final concept, consisting of the three modules: RM1, AXM, and RM2	13
14	Visualisation of code used in locomotion diagram with two examples. (a) RM1 expanded, AXM and RM2 collapsed. (b)RM1 partially expanded, AXM and RM2 expanded	14
15	Explored locomotion sequences. (a) Ideal sequence.(b)First 1 DOF sequence (c)2 DOF sequence (d)Second 1 DOF sequence	15
16	a): Lang Oval tessellation, b): Huffman waterbomb tessellation, c): waterbomb tessellation [10]	18
17	Early sketch of a potential RM using a Lang Hoval tessellation	18
18	Visualisation to show that standard origami creases result in collisions (red), and how creating a channel (green) can prevent this	19
19	Folding pattern for RM module, RED=Mountain fold, BLUE=Valley fold, BLACK=cut . . .	19
20	(a) Picture of the first AXM module design. (b) Picture of the Miuri tube	20
21	(a) Picture of a 5x2 ring with the Huffman star-triangle tessellation. (b) Picture of Huffman star-triangle tube, tessellation is 4x10.	20
22	(a) Picture of a 7 layered collapsable tower dodecagon. (b) Picture of the "Collapsable Tower Dodecagon V2 With Sectioned Folds" without sectioned folds.	21
23	Folding pattern of the AXM module. RED=Valley fold, BLUE=Mountain fold, BLACK=cut	21
24	(a) 3D-printed prototypes of the waterbomb tessellation using living hinges. (b)Mould, ejector, and prototype that was made during this thesis.	22
25	Unfolded waterbomb prototype, made by using clear packaging tape and PLA panels.	23
26	Assembly of an RM prototype, using a stencil to place the panels at the desired location . . .	24
27	Magnet placement for the RM and its resulting simulated behaviour for configuration a,b,c, and d.	25
28	Crease pattern of the RM with magnets, red dots mean the magnet is facing towards the reader, blue dot means the magnet is facing away from the reader.	26
29	Magnet placement for the AXM and its resulting simulated behaviour	27
30	(a)Picture of AXM with too many magnets, which results in a permanent state of collapse.(b) The crease pattern of the working AXM, with magnets (red dots) and panels. Panels in the grey zone are used for the interface between the RM and AXM and are static.	28
31	Picture of the integrated modules with a sketch of the integration piece	28
32	Sketch of setup used during the separate modules experiments	30

33	Results of the quasi-static field experiment for a) the RM module and b) the AXM module. .	31
34	Frames of AXM module being both collapsed and expanded during the quasi-static input experiment. Green: Baseline, Blue: maximum retraction, Red: maximum expansion	32
35	Frames of RM module being both collapsed and expanded during the quasi-static input experiment. Green: Baseline, Blue: maximum retraction, Red: maximum expansion	32
36	Average normalised expansion rate over four cycles for (a): the RM. And (b) the AXM . . .	33
37	Sketch of setup used during the integration experiments.	35
38	Three snapshots of the prototype during the experiment with a cycle length of 0.5 seconds. Displacement over one cycle is displayed with the green and red lines.	36
39	Displacement of prototype after 20 cycles of 0.5 s PD	37
40	Plot of the average velocity as a result of different PDs.	37
41	Plots of the expansion of each module when placed under different phase times. a) PD=0.1 s, b) PD=0.5 s, c) PD=1 s, d) PD=4 s	39
42	Sketch of the potential future design with induction coils.	45
43	a) Sketch of the current hinge system. b) sketch of proposed hinge system for future research	45
44	Sketch of a 1 DOF MSD Model	57
45	Altered MSD model used in this thesis for simulating the individual behaviour of the modules	58
46	Graph visualising difference between model and reality. Blue: Simulation. Black-dashed: Max and Min values of prototype during experiment.	60

List of Tables

1	Design Requirements for origami magnetic capsule robot	9
2	Additional Requirements for the RM	16
3	Additional Requirements for the AXM	16
4	Retraction index of the different magnet placement configurations for the RM module	26
5	Retraction index of the different magnet placement configurations for the AXM module . . .	27
6	Results of the quasi-static input experiments	31
7	Settling times of RM and AXM.	33
8	Absolute results of integration experiments showing expansion of the modules	36
9	Evaluation of all requirements based on final prototype	41
10	Number of parts used in the integration prototype	42
11	Results 50 gsm paper. C=cut, C/G=Almost good engraving but parts are cut, G=good engraving, G/N=There is engraving but it is very shallow, N=no engraving, P=perforation .	56
12	Results 80 gsm paper. C=cut, C/G=Almost good engraving but parts are cut, G=good engraving, G/N=There is engraving but it is very shallow, N=no engraving, P=perforation .	56
13	Parameters used in the MSD model and its real life counterparts	59
14	Parameter values used in simulation	59

2 Introduction

With origami, a complex 3-dimensional object can be created from a simple piece of paper without tearing or glueing. This ancient art form can now also be seen in many engineering projects, as a device capable of completely changing its shape without the need for glueing, welding, or cutting can be very useful, for example, in satellite applications. These need to be compact when launched but as large as possible when in orbit. On a smaller scale, they are contained in airbags that are folded using origami patterns to ensure rapid expansion into the right shape. Going even smaller, origami-based tools are also being developed and used in the healthcare industry. Especially Minimally Invasive Surgery (MIS) benefits from this technology. This surgical discipline aims to perform surgical procedures with minimal incisions. MIS has only been possible since the 1980s, initially made possible by the development of rod lens systems, the reduction in size of video cameras, and specialised surgical tools [28] [37]. However, in the last few decades, cameras have become even smaller, enabling the development of observational capsule robots for use inside the digestive tract or even microscopic cameras on a string capable of traversing the arteries [21] [45]. However, These capsule robots cannot perform any surgical activities and rely on the peristaltic movement of the digestive tract to move the device forward. Some devices are capable of moving by deforming their body, allowing them to aim the camera at a desired location [56]. Such robots that have an elastic body which can be deformed to perform actions are called soft-robots [63].

Having a tool that can alter its shape to be more compact during placement yet be open and functional inside the human body can be very convenient. Making it possible to actuate these tools via a remote magnetic field provides more freedom of movement and makes surgery even less invasive. Soft robots for MIS are already in development, but they are either not endovascular, not magnetically actuated, or do not utilize origami engineering [30] [59]. Thus, this master thesis aims to develop a device that can do all three: be origami-based, magnetically actuated, and useful for endovascular MIS. The endovascular MIS that was chosen as the target for the design of the device was the treatment of Abdominal Aortic Aneurysm (AAA) via Endovascular Repair (EVAR). EVAR is the alternative to open surgical AAA repair and, although safer, is also difficult and requires high precision of the surgeons [32]. Developing a tool that compactly can be inserted inside the aorta and move towards the difficult-to-reach spots could make EVAR less complicated and take less time.

This master's thesis aims to develop a soft robot that can locomote through endovascular systems via magnetic actuation using origami engineering. In Chapter 3, an overview is provided of the design process employed, with a particular focus on the background of origami, the workings of magnetic actuation, and the current state-of-the-art. The chapter ends with a quick introduction to Additive Manufacturing (AM). Chapter 4 sets the boundaries for the design by defining the initial requirements. Within these boundaries, 3 concepts are created, all with a different type of locomotion. The chapter concludes by explaining that all three concepts have flaws and introduces a fourth, final concept. In Chapter 5, this final concept is further defined, providing a more in-depth examination of the method of locomotion and the additional requirements necessary to make this locomotion possible. Following these requirements, various origami patterns, materials, production methods, and magnet placements were explored and selected to define the final design, enabling the creation of a prototype. Chapter 6 and 7 describe the three tests done with the prototype. The first test uses a slow-rising magnetic field as input to determine the maximum expansion rate and gain insight into the folding behaviour of the modules. The second test uses a square wave input to determine the expansion speed of the modules. The final experiment is an integration test of all three modules as a single prototype, enclosed within a tube, as a comprehensive test. These chapters also discuss the results. In Chapter 8, the final design and experimental results are evaluated against the requirements. Going more in-depth about why each requirement was met, why some requirements were not met, and which requirements are inconclusive. The next chapter, Chapter 9, dives in more detail what needs to happen to fulfil the requirements that were not met, how that would come together in one design and the potential use cases for this device. The thesis concludes with a chapter 10 that summarises the process, findings, and limitations of this thesis.

3 Literature research

This chapter presents the background research that formed the basis for the creation of the locomotive device. Research is already being conducted on the subject of origami engineering, as well as medical studies focused on improving and facilitating minimally invasive surgeries. Diving into both topics, as well as finding the right design method and examining the current state of the art, eventually led to a series of requirements that formed the basis for the ideation phase. Additive manufacturing is also briefly discussed.

3.1 Design process

To design a product, a design process is used. Such a design process can be approached in different ways. Corinne Kruger identified four design strategies: Problem driven, Solution driven, Information driven, and Knowledge driven [41]. The most commonly used is the problem-driven design. This method requires the designer to understand the design problem and create a solution around it. Using this approach leads to many requirements being identified and high-quality solutions, however, these solutions are not very creative. A solution-driven design process can be used instead to enhance creativity. The design problem in solution-driven design is poorly defined, only defining when that is needed. This leads to a much larger search space and more varied solutions. The evaluation of these solutions focuses on (re) explaining the problem.

This thesis aims to develop a soft robot utilizing origami and magnetic actuation for MIS. The application of treating an aortic aneurysm is more a guideline than a hard-defined problem and creativity is of utmost importance. Thus instead of hard-defining the requirements to fit an Aortic Aneurysm and following the problem-driven design process. A solution-driven design process will be used.

Problem-driven design and solution-driven design have parallels with the distinction between market-driven and technology-driven innovation in management [34] [19]. Market-driven innovation is innovating based on what customers want, a tool for aortic aneurysms in this case. Technology-driven innovation is when the technology is developed first, where after an application for that is found. In this case, this would be a push to develop a small origami-magnetic actuated locomotion device for inside the human body.

3.2 Origami engineering

The technology that will drive the innovation is the use of magnets to control the folds of origami patterns. Origami is the art of folding paper into a 3d structure. It has existed for hundreds if not thousands of years, with the first books on recreational origami made in the 1800s, but experts believe the art to be much older than that [23] [9].

At the foundation of origami lies the crease pattern, this pattern instructs how to fold the paper to construct the desired shape. One of the best-known origami patterns is the paper aeroplane. Undoing the folds of the aeroplane to transform it back into a piece of paper creates a piece of paper with folding lines, this is a crease pattern. A crease pattern for an origami crane can be found in Fig 1c. The creases are either pointing away or towards the folder. Those folds are called valley and mountain folds, respectively.

A traditional paper airplane is a static origami structure; once folded, the paper stays folded the same. However, dynamic origami also exists; an example of dynamic origami is the paper crane, which, by pulling and pushing its tail, will start to flap its wings. Notice that one translational energy (the tail being pulled) led to rotational energy (wings go down). Origami engineering utilizes this energy translation and flexibility between folding configurations to its advantage, solving engineering problems or creating consumer products [25] [47] [42].

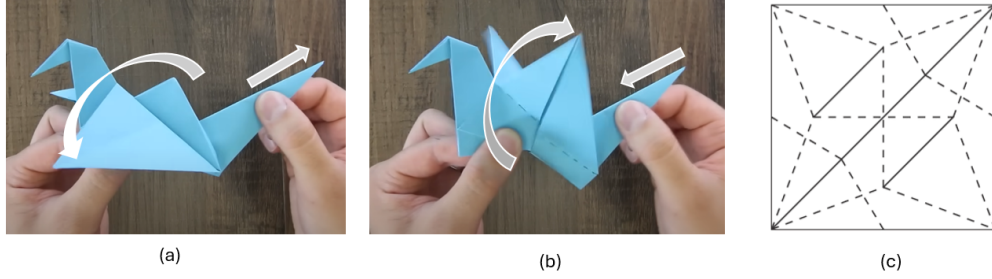


Figure 1: (a) and (b): pictures of origami crane flapping its wings [7]. c: crease pattern of an origami crane, with mountain and valley folds [8]

A better-known application of origami engineering is the solar panels on satellites. During launch, the panels are folded compactly to reduce space. Once the satellite is in orbit, the folds of the solar panel are undone, creating a flat piece of solar panel. When examining images of satellites, the crease pattern is visible, as every separation in the solar panel serves as a hinge or, in origami terms, a fold. Copying this crease pattern onto a sheet of paper allows the shape of the solar panels to be copied; see Fig 2. This figure also shows well how origami patterns work on all scales, without changing the crease pattern. However, origami engineering is not limited to space engineering; it is also used in various products, ranging from airbags to deployable ballistic barriers [18] [55].

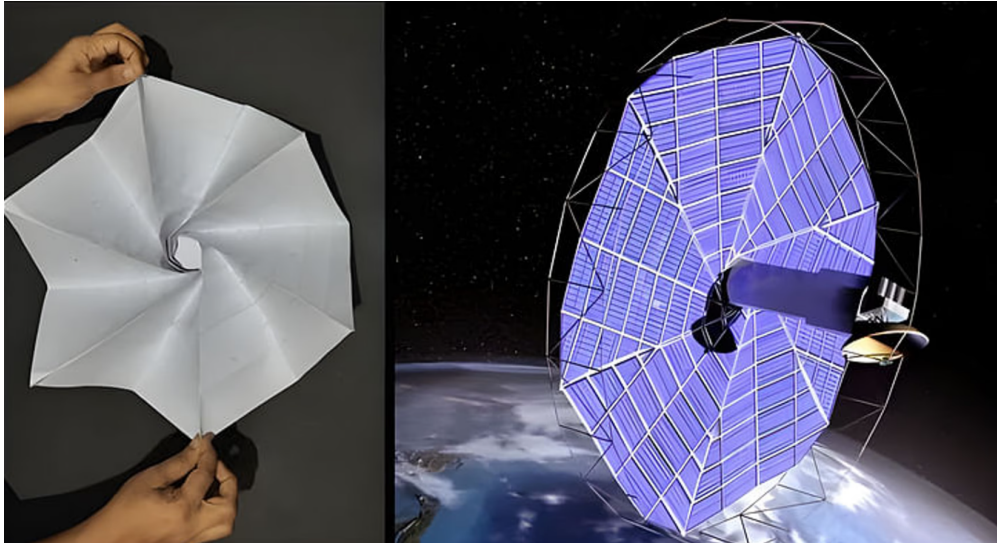


Figure 2: Picture showing how origami engineering is used in satellites and how their crease pattern can be recreated with paper. [3]

3.3 Origami tessellations

Instead of transforming a sheet of paper into different shapes, it is also possible to add folds in such a way as to add structure to the paper. This is done via tessellations, one crease pattern repeated over the entire plane of paper. In Fig 3, the crease pattern for a 3 by 4 (3x4) waterbomb tessellation can be seen.

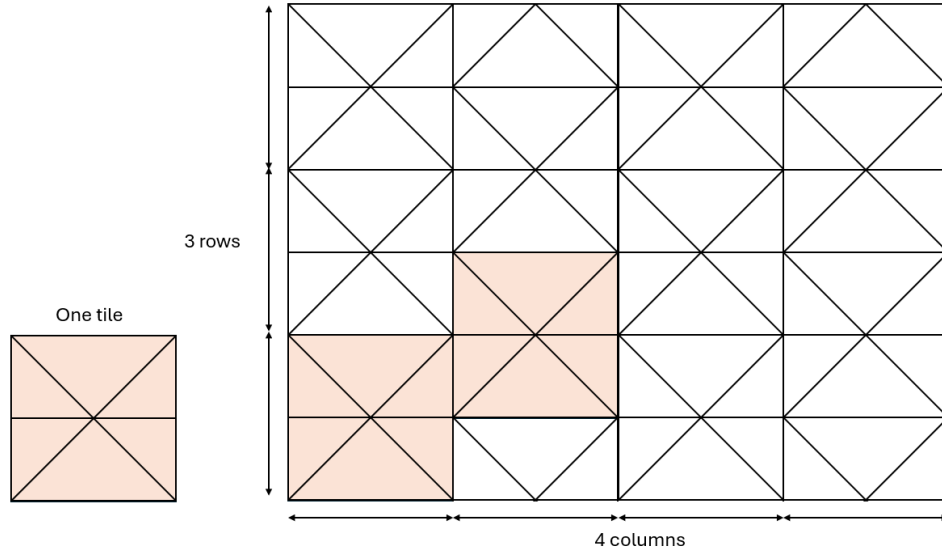


Figure 3: Example of a 3x4 tesseling crease pattern

During this thesis, many tessellations were considered but the most of interest were: The waterbomb, Lang Oval Tessellation, the Hoffman waterbomb, the Hoffman stars-triangles, and The Resch Triangle tessellation. These patterns can be seen in Fig 4. As a dipole magnet inside a uniform magnetic field does not create a force, only a torque (more on this in chapter 3.4), rotations inside the folding pattern, such as the squares in the Hoffman waterbomb tessellation, were a plus. Furthermore, complexity and expansion were taken into account. The most interesting patterns were prototyped using standard origami paper to gain more insights into their workings. Although no conclusion was taken from this analysis, the knowledge about these patterns provided a toolbox for the concept phase.

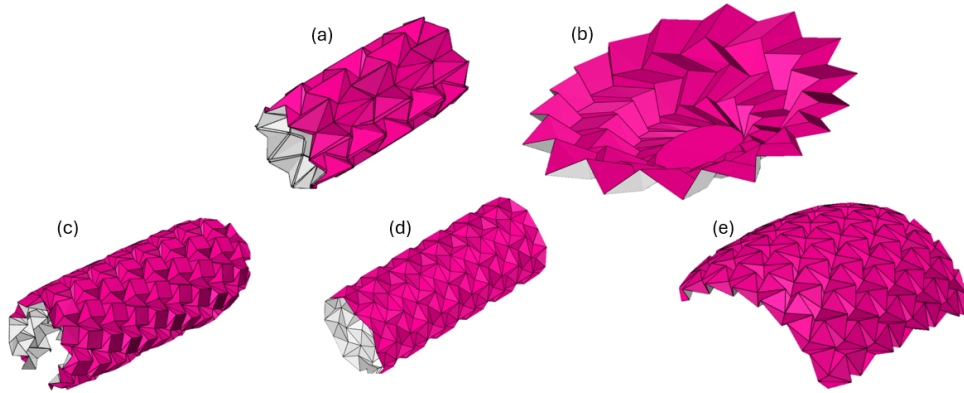


Figure 4: Tessellation patterns of interest for this thesis (a)Waterbomb, (b)Lang Oval Tessellation, (c)Hoffman waterbomb, (d)Hoffman star-triangles,(e)Resch triangle tessellation. [10]

3.4 Magnetic actuation

All dynamic origami has a force that changes the configuration of the origami pattern to increase or decrease certain folds. These can take many shapes: for example motors inside the hinges for satalites [53], an explosion to unfold the airbags or, a hand pulling up the ballistic barrier. The method of changing configuration

in this thesis will be with dipole magnets inside a uniform magnetic field. Dipole magnets are the standard magnets with one south pole and one north pole. When placed inside a uniform magnetic field, dipole magnets want to align with the magnetic field, creating a torque. Counterintuitively, placing a magnet inside such a field does not create a force, meaning that the magnet does not want to move or fly away; it only wants to rotate.

To achieve a uniform magnetic field in this thesis Helmholtz coils are used. This setup consists of two identical electromagnets placed in line with each other. In the area between these two magnets, a close-to-uniform magnetic field is created. An illustration of the forces acting on a dipole magnet inside a uniform magnetic field can be seen in Fig 5.

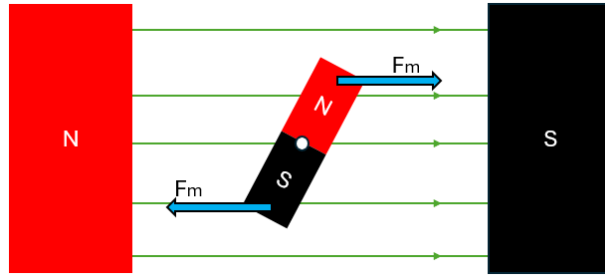


Figure 5: Diagram showing the forces created by the bipolar magnet inside a uniform magnetic field resulting in the rotation of the magnet.

By placing magnets on certain panels of the origami, a torque inside the origami system is created, and the panels with magnets start to rotate. Consider the side view of a simple saw-like origami pattern, as illustrated in Fig 6a. In this scenario, all panels have magnets on them. These magnets are arranged in such a way that when a magnetic field is applied, all magnets want to align with the magnetic field, resulting in the rotation of those panels, see Fig 6b. The result is that the origami structure is now longer, see Fig 6. This principle of using the rotation of magnets inside a magnetic field to collapse or expand an origami structure is the reason the product designed in this thesis is able to be controlled at a distance.

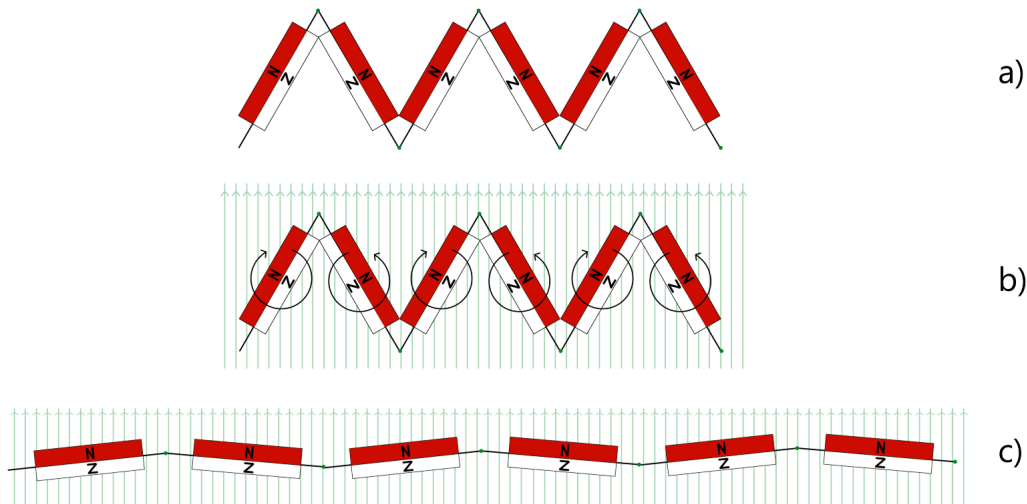


Figure 6: Sketch of how magnets can be used to move origami, with a) being the initial state of the origami. b) showing the forces acting on the initial state of the origami once a magnetic field is applied and c) the resulting end state of origami pattern.

3.5 Living hinges

Paper can easily be folded; however, in this thesis, plastic is considered as an alternative material. Creating creases such that an otherwise stiff plastic material can fold has been in use for many years. Such a crease is called a living hinge and there are many types of living hinges. An example of a common living hinge is the hinge keeping the shampoo bottle and its cap connected. The plastic of the hinge, the top of the bottle, and the cap are all the same. However, only the hinge can be folded. This is done by making the crease less thick than the other region and is one of the simplest forms of a living hinge. More interesting patterns emerge with the other material living hinges are used, wood. Kits to create miniatures make use of living hinges to bend the normally straight pieces of wood in organic curves [5]. An example of such a kit and inspiration for this thesis can be found in Fig 7.

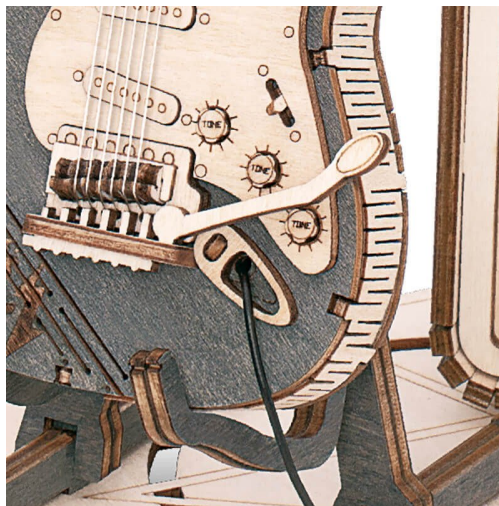


Figure 7: Living hinges as used in the Robotime electric guitar [11]

3.6 AAA

An AAA is a widening of the abdominal Aorta. When the aorta has a dilation in diameter of at least 50 % relative to its expected diameter it is defined as an AAA [40]. Estimates on prevalence lie between 1 and 12 %, with a median of 5 % [57]. However, this number increases to 8 % for men above 65 years [49]. There are also a lot of deaths due to AAA. In the USA alone 6.300 people die every year due to complications from AAA [57].

There are two methods of treating AAA, open surgical AAA repair and EVAR. EVAR has been on the scene since the 1990s and is considered the preferred method of treating AAA, due to its lower mortality rate [32]. The treatment is a minimally invasive surgery (MIS) where a stent is positioned to the aneurysm via the leg. This stent reduces the pressure on the aortic wall and thus prevents the aortic wall from bursting. EVAR uses less anaesthesia and reduces complications in patients with chronic obstructive pulmonary disease and or kidney disease; however, when an aneurysm does not fulfil specific standards, an open surgical repair has to be done. This treatment, introduced in the 1950s, consists of the surgeon opening the chest of the patient, opening the aorta and sewing a tube similar in shape and size to a healthy aorta inside the aneurysm. This procedure is more intensive for the patient and takes longer than EVAR, but is needed if EVAR is no option.

A third treatment method using drugs has been in development over the past few years. However, as this method's effectiveness is currently seen as controversial or inconclusive, it is not taken into account for this thesis [44]. The focus of this paper will be on making the EVAR procedure more easy and reducing the time of operation. One of the major difficulties during the procedure is placing the guidewire in side arteries [58]. This is currently done with a long wire and takes skill and patience to do correctly. The design proposed in this thesis could provide an easier alternative.

3.7 State of the art

Origami robots to be used inside the human body for medical applications do exist. For example, a magnetically actuated origami robot designed to be ingested. The little robot would expand inside the stomach and with the magnetic fields would be controlled to carry out underwater manoeuvres to remove a button battery, burned inside the stomach [46].

Another origami robot for the digestive tract is the capsule endoscope which can be seen in Fig 8a. This design uses origami to control the direction of movement; when the origami pattern is folded, the capsule is propelled forward through the intestinal peristalsis. When the structure is unfolded the origami structure causes the intestinal peristalsis to push the capsule in the opposite direction, although the method of controlling the origami has not been tested, one of the proposals is to actuate the origami via a magnetic field [30].

These examples show how magnetic actuated origami can be used in practice. A more conceptual method is the magnetic origami spring robotic system. This device uses the torque created by two permanent magnets inside a uniform magnetic field to expand and collapse an origami structure [65].

The lack of origami capsule robot devices for endovascular systems suggests that origami might not be a good solution or even possible inside the endovascular system. However, an intracardiac magnetic resonance imaging (ICMRI) catheter was redesigned using origami. The system not only became more compact the new design showed improvements [59]. The structure was, however, not actuated via a magnetic field, as that would disrupt the magnetic resonance imaging.

The last device to mention in this state-of-the-art section is the master thesis of G.M. van Vliet. The device has fins on the outside of the capsule positioned as the thread of a screw. The idea is that when the capsule is rotated, it moves forward through the aorta like a bolt moving through a nut. The system, however, damages the aorta too much, potentially due to sliding and the fins being too stiff. [61].

These devices were put inside a Venn diagram, see Fig 8. This Venn diagram shows clearly the problem with the current state of the art. A device that is origami-based and has magnetic actuation, and is designed for endovascular use seems to not yet have been proposed. There are however already devices that have 2 of the 3 traits, which can be used as inspiration.

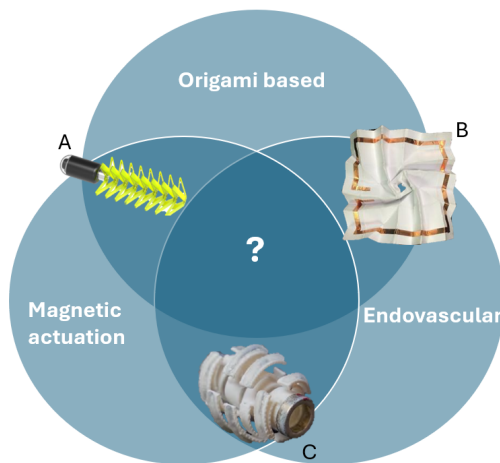


Figure 8: Venn Diagram visualising the current state of the art of magnetically actuated, origami-based, endovascular devices. A: Magnetically actuated, origami-inspired endoscope capsule. B: Origami-based ICMRI catheter. C: Compliant magnetic capsule robot to traverse the aorta. [30] [59] [61]

3.8 Additive Manufacturing

Additive Manufacturing (AM), better known as 3D printing, is a relatively new production process that formerly was known as rapid prototyping. Over the years users realised that this technology has more uses than only rapid prototyping and was thus rebranded to additive manufacturing [31]. There are different types of AM machines but all create a product by adding material, thus the name additive manufacturing.

To produce an object using AM an object is made in 3d software. This object is converted to a stereolithography (STL) file approximating the object made in the 3d software with triangles. Using slicer software, the STL file is then sliced into layers with each layer containing the information of how that specific layer needs to be printed [62]. The 3d printer then prints each of those layers one by one resulting in a physical version of the digitally drawn object.

One of the reasons additive manufacturing fits so well in this thesis is that developing a scaled-up or scaled-down version of an object is easy. This makes additive manufacturing a good match with origami, which can also be scaled to any size without much problem. As mentioned earlier, many different versions of AM exist. The most common is the FDM printer, based on melting a solid so it can be placed on the printer bed. But other versions are based on the polymerisation of a liquid using light or melting powder particles together using a high-powered laser [29] [54]. In this thesis, the FDM printer "Bambu Lab A1 mini" will be used to produce parts for the prototype.

4 Preliminary Design

In this chapter, the preliminary design will be discussed. Based on the state of the art and the design problem, this project's requirements were set as design boundaries. This is followed by the concept development and the decisions that lead to the final design.

4.1 Requirements

Nine requirements were created based on the problem described in the introduction and the devices brought forward in the state of the art. This chapter will detail these requirements, but a summary can be found in Table 1.

Table 1: Design Requirements for origami magnetic capsule robot

Requirements	Description
R1 Outer diameter adaptability	Outer diameter must be able to fluctuate 16 %.
R2 Aortic wall safety	Pressure generated must not rupture the aorta.
R3 Locomotion	System must move through the aorta in a controlled manner.
R4 Continued blood flow	System must allow blood flow and reduce pressure drop.
R5 Failure rate	Design must be simple yet strong enough to reduce chance of failure.
R6 Biocompatibility	Material and shape must not induce an immune reaction in the body.
R7 Simplicity	For production and failure rate as few parts as possible must be used.
R8 Origami Engineering	Design must make use of origami engineering to find a solution.
R9 Magnetic actuation	Design must be controlled wirelessly via magnetic actuation.

Outer diameter adaptability (R1) - The diameter of the Aorta fluctuates dynamically due to the cardiac cycle and statically due to the building structure of the aorta. A 2019 study investigated these fluctuations [36]. By taking the maximum diameter of the aorta (proximal-Asc) during diastole (34.10 mm) and the minimum diameter (distal-asc) during systole (28.77 mm) and normalising these two values, the factor for how much the diameter must be able to contract is 0.84. Thus, the concept must have an outer diameter of 31.44mm and at least be able to adjust its outer diameter with $\pm 8\%$.

Aorta wall safety (R2) - A burst in the aortic wall would be catastrophic; Bogdan Cizek et al. found that the burst pressure of the aortic wall was, on average, $2.24E5 \text{ N/m}^2$ with the outer limits being $1.14E5$ and $4.36E5 \text{ N/m}^2$ [20]. With a little safety margin in mind, considering the system is still a prototype, a maximum of $1.0E5 \text{ N/m}^2$ is set as a requirement.

Locomotion (R3) - Navigation of the robot is an important part of the design; the robot should be able to displace its own centre of mass through an aorta like structure.

Continued blood flow (R4) - The aorta is a crucial component of the blood circulation system, and the impact of this robot on blood flow should be mitigated. A 2022 study [15] simulated different blockages of the aorta and found that a blockage of over 35 % had a significant impact on blood pressure. A maximum blockage of 35 % will be set as the goal; however, further research will be required to calculate the maximum allowed pressure drop.

Failure rate (R5) - As the aorta is such an important part of the human body a failure of the capsule of any sort can be catastrophic and cost a human life. The exact failure frequency does not matter yet, as this can not be tested during this thesis. The requirement is, however, still taken into account during the design process and must be as low as possible.

Biocompatibility (R6) - The immune system of a human body does not like foreign objects. Although the capsule is not meant to be in the human body for long periods, the immune system should not activate or

attack the capsule. To do this, a coating can be used of biocompatible material, and sharp edges must be reduced to the bare minimum.

Simplicity (R7) - A simple design is often the best, in this thesis that is for two reasons. First, fewer parts mean fewer points of failure. So, to keep the failure rate as low, the design must have as few parts as possible. Second, every extra step that is needed in the production process because of extra parts costs time and increases the chance of errors happening during production. Overall, there is no hard limit to the maximum number of parts allowed, but as a guideline, the thesis aims to keep the number of parts below 100.

Use origami engineering (R8) - The goal of this research is to set a step forward in origami engineering for MIS. The knowledge gained by developing this system with origami engineering is thus valuable.

Use only magnetic actuation (R9) - Although the system will most likely pull a guidewire, it must be wirelessly controlled only by adjusting a uniform magnetic field in which it is placed.

4.2 Ideation

Following the requirements and the state of art analysis. Four key variables were defined. Method of locomotion, Aortic adaptability, base structure of the design, and method of actuation. These variables were put in a morphological diagram and for each variable, at least three solutions were found. This diagram can be found in appendix 11.1. Parallel to that insight into existing tessellating origami patterns was investigated via literature research. These origami patterns were graded on their potential use, with the best ones continuing into the concept phase.

4.3 Concepts

The concept phase included developing three concepts. These were derived from the morphological chart described in the previous chapter. These concepts all use a different method of locomotion and were deliberately designed to be as unique as possible.

4.3.1 Self-propelled vine robot

The first uses the treadmill method for locomotion. This solution was inspired by the vine robot developed in 2020 by researchers at Stanford University [22], this robot can locomote by expanding its tip without having to move itself. It does so by feeding itself new material via the inside. It should be possible however to feed itself just as Toroflux, a toy from 2010 [35]. And as it happens such a robot was presented in 2022 that used this technique with an internal robot [52]. This proves that this is a valid locomotion technique. The self-propelled vine robot concept also uses the inflated tube system, to adjust its radius to the desired value. Using the origami kaleidocycle pattern was also considered, this pattern can be seen in Fig 9. However, as this pattern would be more difficult to expand or retract radially was not chosen over the inflated tube. The self-propelled vine robot would be actuated by placing small magnets on the tube; by oscillating a magnetic field at just the right time, the system would move in the desired direction. A sketch of the concept can be found in Fig 10.

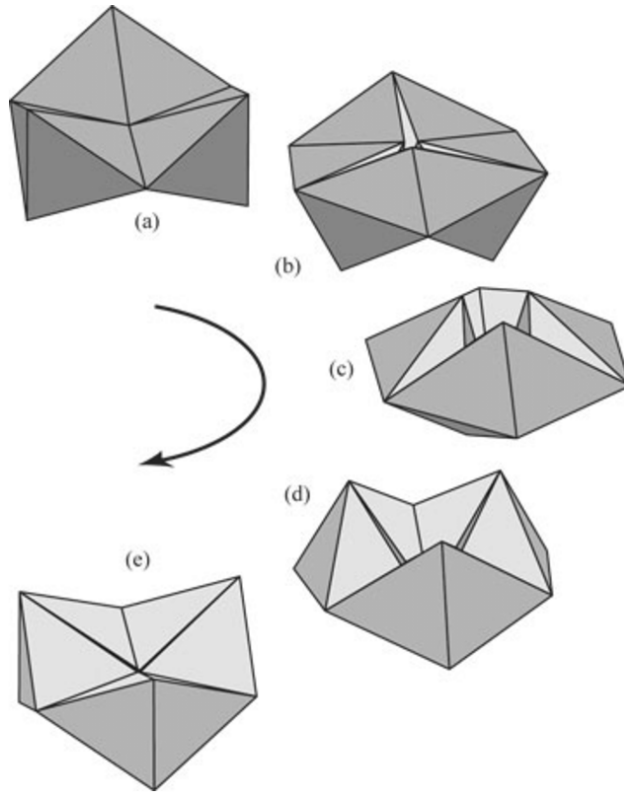


Figure 9: Step-by-step visualisation of the working of the koleidocycle, starting with (a), then (b), until (e). After (e) the cycle starts again with (a). [26]

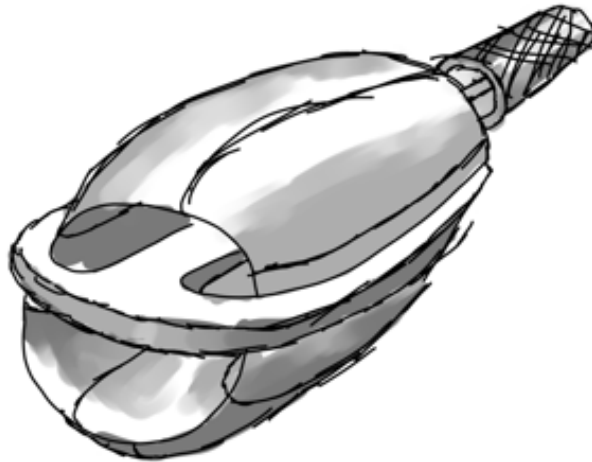


Figure 10: Sketch of the self-propelled vine robot pulling a stent

4.3.2 Popping screwthread

The second concept was inspired by the screw design of G.M. van Vliet [61]. His device rotates axially through the arteries, and fins on the outside of this device slide the device forward as a bolt sliding through

a nut. The popping screwthread concept uses the same locomotion method. Having a body that rotates axially with fins on the outside. However, instead of rigid fins, these fins can collapse for easier placement and retrieval from the human body, and more subtle actuation prevents damage from happening on the arteries. A sketch of this method can be found in Fig 11.

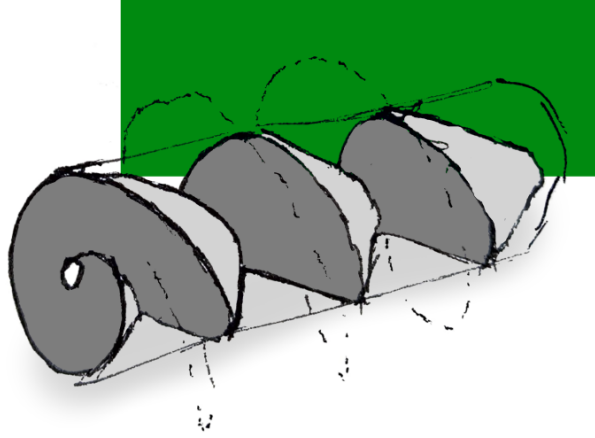


Figure 11: Sketch of the popping screwthread concept

4.3.3 Negative-poison ratio worm

The last concept was the negative poison ratio worm, inspired by a paper exploring negative poison ratio origami structures to create a worm-like robot [27]. A negative Poisson ratio structure becomes wider as you lengthen it. Most objects, when stretched in one direction, contract perpendicular to this force. A good example would be a rubber band, which, when pulled, becomes thinner. A negative Poisson ratio object does the opposite; when stretched in one direction, it expands perpendicular to this force. Making it look similar to a balloon.

The previously mentioned paper adds several of these negative Poisson ratio origami structures next to each other and is able to control them separately. This allows the researchers to create a wormlike peristalsis movement. However, the researchers use motors to actuate these structures which is not possible for the purpose of this thesis. So this concept is a scaled-down version of that worm with magnets actuating the waterbomb origami structure. A concept sketch was made and can be seen in Fig 12. It consists of 6 modules that have a negative poison ratio, 3 are inflated in a positive magnetic field, and the other 3 are collapsed inside the magnetic field. This switches when the magnetic field is inverted.

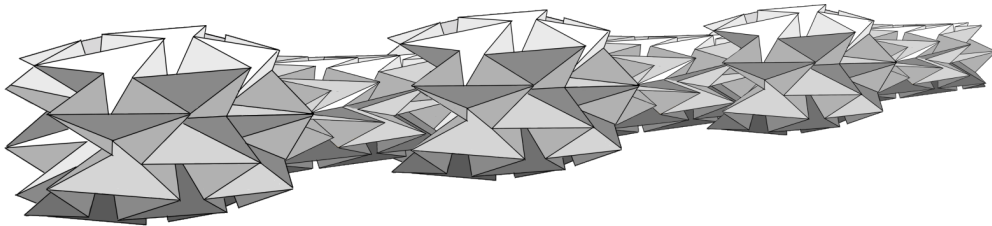


Figure 12: Early concept sketch of the Negative-poison ratio worm, consisting of 6 identical modules.

4.4 Choosing a concept to continue

The first concept to fall was the screw thread concept. This is because in the discussion of his research, Vliet brings up that the device will most likely heavily damage the aorta, he proposes several reasons, the

device has too much surface roughness, too high stiffness in the fins and/or low compliance with the aortic wall. The popping screwthread concept would most likely encounter the same problems. Although these could potentially be solved by optimising the material and dimensions, the other two concepts do not require sliding over the aortic wall and thus are assumed to be a lot less damaging.

Choosing between the vine and worm concepts was more challenging. However, due to its complexity in integrating origami and the lack of a clear method to reduce its outer diameter, the vine concept was also scrapped. This left only the worm robot. But with the first few paper prototypes made, the problem arose that although the waterbomb did expand 2.5 times radially, it only expanded 1.01 times axially. This minimal expansion axially would not allow for proper locomotion. This happened due to a misinterpretation of the original worm paper, which would not be discovered until much later in the thesis.

This discrepancy in expansion would however hold the key to the final design. As the waterbomb has a near 0 expansion axially then by adding a module which almost does not expand radially but does expand axially the same locomotion is possible. This solution also, almost paradoxically, allows for fewer modules to be used. As for locomotion, only three modules would be needed; two modules that alternate to grip the wall of the aorta, and one module that displaces the module that has no grip. For visualisation, a sketch of this final concept can be seen in Fig 13.

The two modules that alternate with grip on the aorta need to expand radially and will be referred to as the First Radial Module (RM1) and Second Radial Module (RM2). Radial Module (RM) is used when non-specifically referring to either RM1 or RM2. Connecting and displacing the RM's is a module that needs to be able to expand axially, so this module will be referred to as Axial Module (AXM).

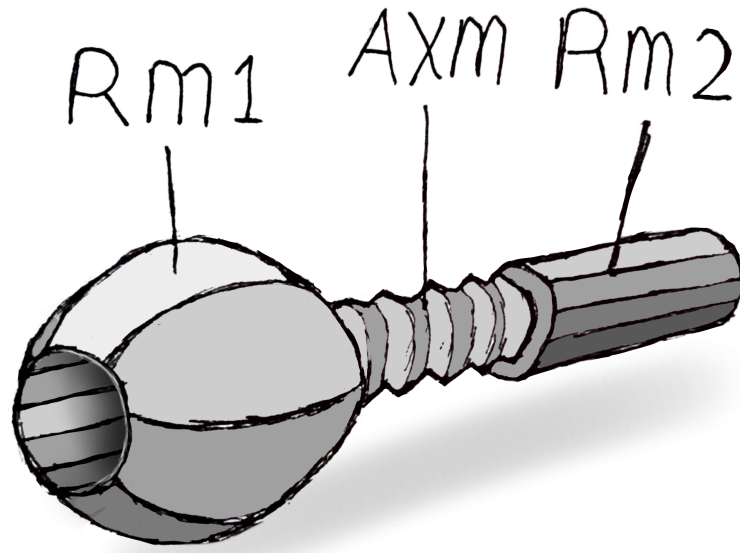


Figure 13: Sketch of the final concept, consisting of the three modules: RM1, AXM, and RM2

4.5 Conclusion of preliminary design

Based on the state of the art and the design problem, 9 requirements were established. Different solutions for these requirements were put inside a morphological diagram. These solutions were used to develop three different concepts: 'the self-propelled vine-robot', 'the popping screwthread', and 'the negative poison ratio worm'. Each was analysed on its applicability, but the best concept to continue with was chosen to be the 'negative poison ratio worm', as this concept had a lesser chance to damage the aorta relative to the 'popping screwthread' concept and is less complex than the 'self-propelled vine-robot'. The worm concept, which consisted of 6 identical modules that expand both radially and axially, was simplified to 2 radially expanding modules and 1 axially expanding module. This new design is the concept that was used in the continuation of this thesis.

5 Final design

The final design consists of three parts: two modules that can expand radially connected by one module that can expand axially, as sketched in Figure 13.

This chapter starts with a deeper analysis of the locomotion methods that are possible with this setup. After that, additional requirements are described per module because to make this new design and locomotion method work, additional requirements are needed. These requirements and the first prototypes lead to decisions in origami pattern, magnet placement, and material, which will be described in detail at the end of this chapter.

5.1 Locomotion

To determine how the device would move, first, the ideal, sequence of expansions was identified, determining what sequence would be ideal if there were no limitations. Assuming all modules are collapsed, first, RM1 expands and clamps the aorta. Then AXM pushes RM2 forward. When RM2 is in place it expands and clamps. RM1 is then deflated which, when fully deflated, is pulled towards RM2 by the retracting AXM. This process is repeated until the device is at the desired location.

Different sequences have been explored and put in a locomotion diagram which can be seen in Fig 15. In the diagram all 3 segments are assigned a number between 0 and 1 correlated to the state of that module so 1-0-0 should be read RM1 = fully extended. AXM and RM2 are totally collapsed. This coding is visualised in Fig 14. The colour code of the locomotion diagram is as follows: the purple and green squares indicate whether the magnetic field is positive or negative. The red border indicates that the field is using conduction to heat up a desired part, where as the blue border indicates it has been turned off.

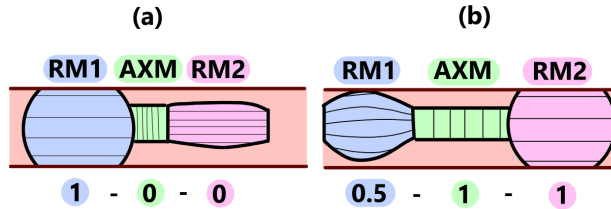


Figure 14: Visualisation of code used in locomotion diagram with two examples. (a) RM1 expanded, AXM and RM2 collapsed. (b) RM1 partially expanded, AXM and RM2 expanded

Ideal sequence Fig 15a. shows the ideal 3 DOF no constriction pattern.

First 1 DOF sequence Pattern B was the first attempt at a 1 DOF sequence. All segments open when put under the same magnetic field; however, with different stiffness and dampings, a delay causes the first to be opened, then the second and at last, the third. When put under an inverse magnetic field, this once again happens, but in reverse, the first one closes, then the second and at last, the third. This sequence pushes RM2 when RM1 has a grip and retracts RM1 when RM2 has a grip so the device will displace. However, this method has a downfall; during the cycle, there is a moment in which both the first and third segments are not clamping. As this could result in the robot moving with the bloodstream this is not desired.

2 DOF sequence The next step was to add a DOF. This was done by adding an induction coil that heats the creases of the AXM; if the ASM is made of memory-shaped polymer, the segment can be turned on to react to the magnetic field. this can be seen in Fig 15c. Assume RM1 and AXM open during a positive magnetic field while RM2 closes under the same field. However, AXM only changes state if the induction coils heat up the creases of the module. A method of locomotion is as follows, starting with a positive magnetic field without induction, RM1 opens without AXM. Then AXM is heated up and folds open under the already present magnetic field. It is then cooled the hinge stiffens once again. The magnetic field then switches causing RM1 to collapse and RM2 to open. AXM remains open as it is stiff. When RM2 has grip, AXM is heated which causes it to close under the magnetic field and pulls RM1 to RM2. AXM is cooled, and the magnetic field becomes positive again, after which the cycle repeats. This method would work but the

usage of MSP adds complexity to the device, which increases failure modes and the complexity of reducing its size.

Second 1 DOF sequence The final method D, was done by assuming different expansion speeds for different modules. Specifically, AXM opens and closes much slower than RM1 and RM2. The cycle would be as follows. The magnetic field starts positive opening RM1 and AXM. However, when AXM is at full expansion and gets traction AXM is not nearly done with expanding and pushes with the remaining time RM2 forward. Then the magnetic field is inversed and RM1 and RM2 quickly switch states. AXM, which is still slower, pulls once RM2 gets traction segment one to RM2. This then repeats over and over. In this example, AXM is quicker than RM1 and RM2. However, as long as these speeds are not the same, the technique should work; inversing (so RM1 and RM2 are quicker than AXM) would make the device move backwards. But as there is no front or back yet to the device, as long as the expansion speeds are not equal, the system should move.



Figure 15: Explored locomotion sequences. (a) Ideal sequence. (b) First 1 DOF sequence (c) 2 DOF sequence (d) Second 1 DOF sequence

5.2 Additional Requirements

Table 2: Additional Requirements for the RM

Requirements for RM		Description
rm-R1	Radial expansion	For locomotion device needs to expand 2x radially
rm-R2	No axial expansion	For simplicity no axial expansion is preferred
rm-R3	Module interface	The module must be able to connect to the AXM
rm-R4	Field along symmetry axis	Actuation only possible via magnetic field along symmetry axis
rm-R5	Quick expansion	Needs to expand and retract quicker than the AXM

Table 3: Additional Requirements for the AXM

Requirements for AXM		Description
axm-R1	Axial expansion	Needs to expand and retract axially to enable locomotion
axm-R2	No radial expansion	For simplicity no radial expansion is preferred
axm-R3	Module interface	The module must be able to connect to the RM
axm-R4	Field along symmetry axis	Actuation only possible via magnetic field along symmetry axis
axm-R5	Slow expansion	Needs to expand and retract slower than the RM

To enable this final design and locomotion technique, additional requirements were set up. The requirements can be found in Table 2 and Table 3, in this chapter these added the details of these requirements can be found. It is important to make clear that these requirements are in addition to requirements found in Table 1, the original requirements are still valid.

5.2.1 Requirements for RM

Radial Expansion (rm-1) - This requirement at a glance seems very similar to requirement R1 Outer diameter adaptability. But the reasoning and fluctuation value are very different. To enable locomotion, the RM needs to expand and retract radially. This is explained in chapter 5.1. This means that when the RM is expanded and gripping the wall, it needs to retract at least 16% to be certain that the RM has no more contact with the aortic walls. Calculated as follows

$$1 - \frac{\text{min. radius aorta}}{\text{max. radius aorta}} = > 1 - \frac{28.77}{34.10} = 15.63\% \approx 16\% \quad (1)$$

. In this thesis, the expansion value is used more commonly, similarly calculated as the retraction value, but switching the numerator and denominator to the lowest expansion value to be certain that the RM touches the aorta is 19 %. To be certain the device does not slide along the aorta an ambitious but possible expansion value of 100 % (or retraction value of 50 %) was set as a goal and requirement.

No axial expansion (rm-R2) - Why no axial expansion is required for the RM module can best be explained by analysing what would happen if there was axial expansion. If the device is seen as one unit, the axial expansion is not a problem; the axial expansion of RM1 would, in theory, cancel out with the axial retraction of RM2. However, analysing at a modular scale it can be seen that the AXM is now rocking unnecessarily between the two RMs. This is not only a loss of energy but could also increase the failure rate of the interfaces between the modules.

Module interface (rm-R3) - This requirement is more straightforward than the previous requirements. The RM module needs to be able to connect to the AXM module.

Field along the symmetry axis (rm-R4) - The final design requires the RM to expand in all radial directions simultaneously. A method to achieve this is to make the device radially symmetric just like for example

a snowflake. Then with magnets on the origami pannels have a magnetic field run straight through the heart of the snowflake. This means that every arm (for the lack of a better word) of the snowflake receives the same magnetic field and thus should expand or retract in perfect synchrony. Something to note is that more arms are better, as the force is more evenly distributed and deviations in expansion between arms (due to production error for example) are less noticeable. However a minimum number of arms is not set as requirement as the device would work with both 3 arms or with 50. Just possibly without the previously mentioned advantages of having more arms.

Quick expansion (rm-R5) - As described in section 5.1 the locomotion method uses the difference in expansion speed between the RM and the AXM to generate displacement of the device. As the AXM needs to displace RM2 and thus has more inertia, and needs to expand over a larger distance. The goal is to have the RM be quicker in expansion than the AXM

5.2.2 Requirements for AXM

Axial Expansion (axm-R1) - The method of locomotion relies on the axial expansion of the AXM. Although, in theory, any expansion above 0 % would be enough for locomotion, a low expansion rate would require more cycles for the same displacement with a larger expansion rate. A target rate of 100 % expansion, or 50 % reduction, is set as a target for this thesis.

No radial expansion (axm-R2) - Radial expansion inside the AXM means more displacements and, thus, more energy loss. Making the device less efficient and prone to a higher failure rate.

Module interface (axm-R3) - The AXM needs to connect to the RM on both sides and thus needs 2 interfaces for the other modules.

Field along symmetry axis (axm-R4) - Although on its own the AXM does not need this requirement. The RM requires it, thus the AXM has no other choice than to do the same.

Slow expansion (axm-R5) - See 'Quick expansion (rm-R5)' for the explanation of why the AXM needs to be slower than the RM.

5.3 Origami patterns

After the defining of these requirements, different origami patterns were explored and optimised.

5.3.1 Origami pattern for RM

For the RM, different patterns were explored, but the three most interesting patterns were The waterbomb, the Lang Oval tessellation, and Huffman's waterbomb. These patterns can be found in Fig. 16. Starting with the Lang Oval Tessellation, two of these patterns would be connected via rods. The static core of the pattern would allow for an easy interface between modules, but due to the limited expansion rate and overall complex design, the Lang Oval Tessellation was discarded. An early sketch of this concept can be seen in Fig 17

The Huffman waterbomb was a pattern of interest as the rotating squares would make actuation via magnetic torque straightforward. However, there are many places in this pattern where the paper needs to make several 180° bends in a row. The thicker the material, the more difficult it is to make these bends. Due to this, the Huffman waterbomb was discarded as well.

This leaves only the waterbomb in the race. Glueing the waterbomb pattern into a tube creates two holes (or one if you study topology), which stay constant in radius. This is ideal for interfacing with the AXM. The first prototypes during Ideation showed no axial expansion which is also a requirement fulfilled. By adjusting the number of tiles, the expansion rate and the sharpness of the angles can be controlled. Previous research used 3x8 tessellation [27]. However, this would expand one column completely. For the magnetic actuation method, this is not handy as a more complete expansion allows better use of the magnets. An

additional column was added as well to increase the expansion rate but still allow the pattern to fit on an A4 paper. So the final tessellation size is 4x9.

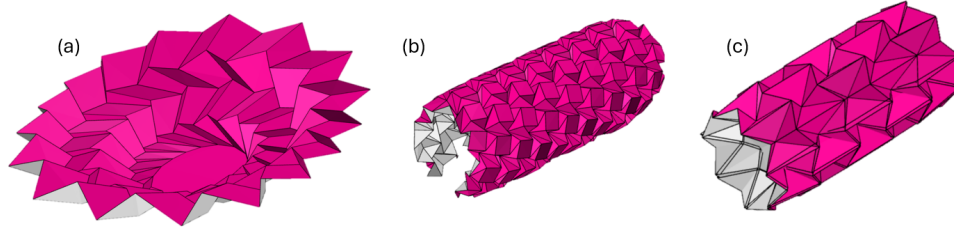


Figure 16: a): Lang Oval tessellation, b): Huffman waterbomb tessellation, c): waterbomb tessellation [10]

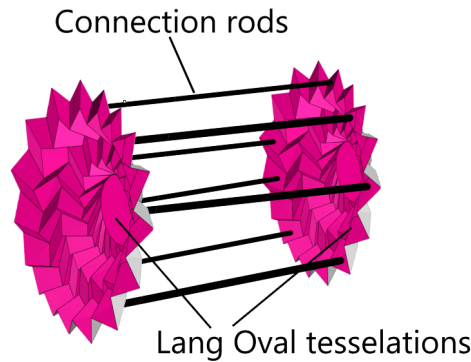


Figure 17: Early sketch of a potential RM using a Lang Oval tessellation

Using these fold lines results in a proper waterbomb. However, every plane will get a thickness thicker than paper. The reason for this will be explained in chapter 5.4 Material. This thickness creates a problem for valley-folds as the two panels glued on top will collide, see Fig 18a. There are different solutions, using offset hinges to create one hinge, for example, [43]. Methodologies for creating thick-panelled origami patterns do exist [50] [51]. Applying these methodologies was, however, out of the scope of this research. As the offset hinges add too much complexity, a different solution was used. Every hinge was replaced by two hinges, with a channel between them. The difference can be seen in Fig 18b. This method is far from perfect and is only possible because of the flexibility of paper which creates where necessary additional fold lines. This additional bending does make the system less energy efficient and makes the device prone to a-symmetry leading to unwanted behaviour. Where the channels intersect, a hole is made; this reduces stiffness and provides flexibility when imperfect folds occur. The final crease pattern for the RM can be found in Fig 19.

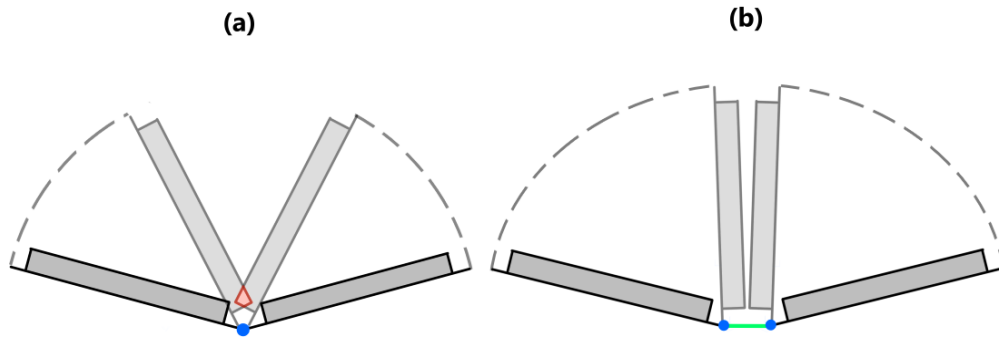


Figure 18: Visualisation to show that standard origami creases result in collisions (red), and how creating a channel (green) can prevent this

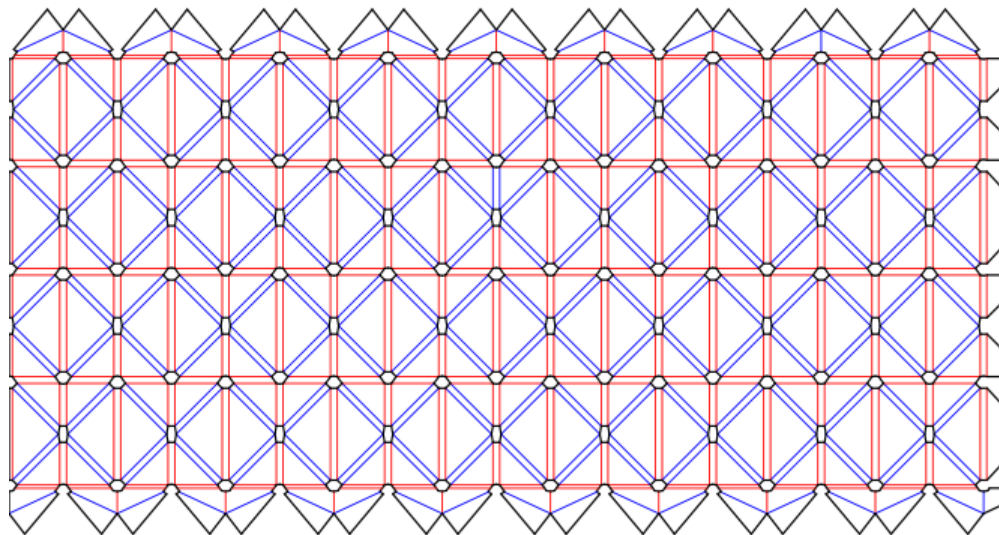


Figure 19: Folding pattern for RM module, RED=Mountain fold, BLUE=Valley fold, BLACK=cut

5.3.2 Origami pattern for AXM

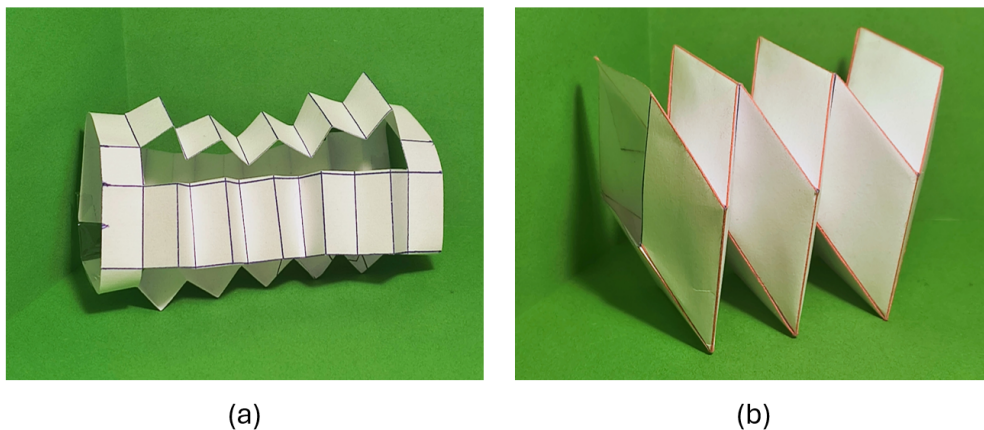


Figure 20: (a) Picture of the first AXM module design. (b) Picture of the Miuri tube

The design of the AXM started in its simplest form, with 4 jigsaw folded arms separately connecting the two other modules. A picture of this design can be found in Fig 20a. This design, however, is unstable. Although either retraction or expansion can be easily achieved with magnets. Both are not possible.

With the focus on stability, the next origami pattern explored was the Miuri tube. This tube can be seen in Fig 20b. This pattern is a lot more stable than the first version. However, since it has planar symmetry rather than radial symmetry, it is challenging to place magnets; however, this also causes the ends of the tube not to remain static. Which makes connecting the AXM to an RM difficult.

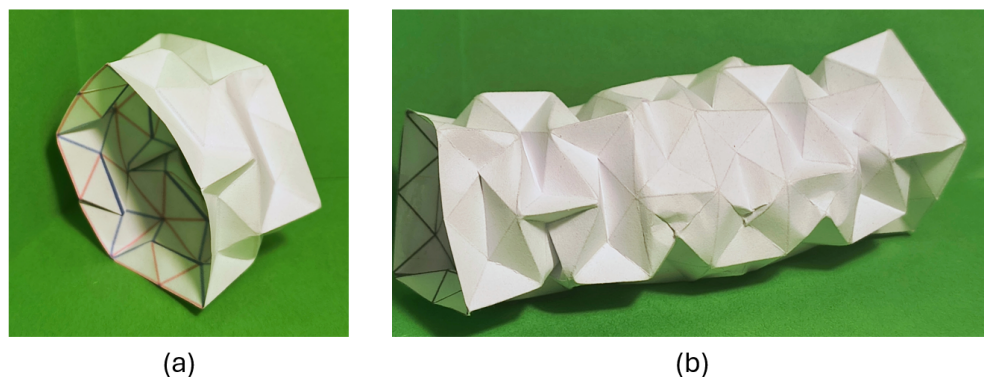


Figure 21: (a) Picture of a 5x2 ring with the Huffman star-triangle tessellation. (b) Picture of Huffman star-triangle tube, tessellation is 4x10.

During the exploration of RM designs, the Huffman star-triangle tessellation was discovered. On origamisimulator.org, this pattern is folded in a tube without any axial expansion. First, several rings with varying numbers of tessellations were created to determine if the pattern could be useful. Such a ring can be found in Fig 21a. With a theoretical expansion rate of 100 %, this seemed perfect. Some small-scale magnet studies have already been conducted on separate tiles of this pattern, with success. However, when attempting to extend the ring to a tube, the entire tube became too unstable and stiff; a picture of this tube can be seen in Fig. 21b. Thus, this design was also discarded.

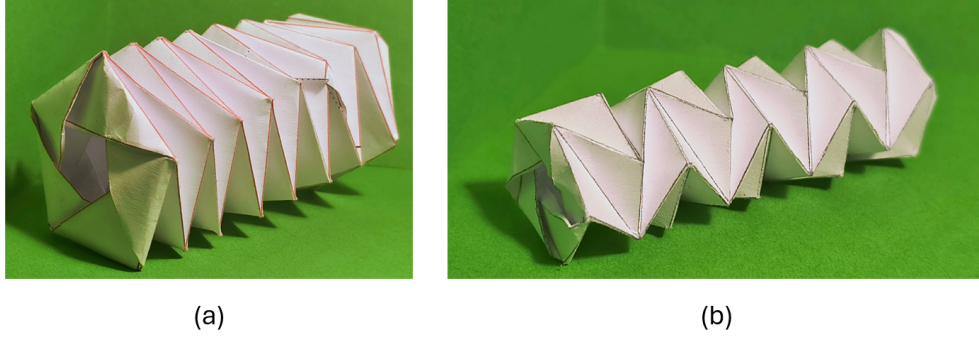


Figure 22: (a) Picture of a 7 layered collapsable tower dodecagon. (b) Picture of the "Collapsible Tower Dodecagon V2 With Sectioned Folds" without sectioned folds.

This leads to the pattern that would be used in the final design of the "Collapsible Tower Dodecagon" [1]. This pattern showed a stable tube design with a static bottom and top, making it ideal for interfacing. The paper prototype, as shown in Fig. 22a, had an expansion rate of approximately 300 %. However, as the AXM expands, the ends rotate with respect to each other. This is undesired, as the rotation of one of the RM's could damage the aortic wall and require additional energy. However, the "Collapsible Tower Dodecagon V2 With Sectioned Folds" [2] came with a solution by mirroring every layer. The rotation of the ends is net zero. Meaning that the RMs will not rotate with respect to each other. The sectioned folds, however, were not necessary, so these were removed without any issue. The resulting tube can be seen in Fig 22b. This design is currently being researched for its impact mitigation capabilities; in this context, the fold is referred to as a Triangulated Cylindrical Origami [64]. This thesis will, however, keep using the name Collapsible Tower.

The folding pattern still has the same problem as the RM. That is, 180-degree valley folds are not possible with thicker paper. Thus, channels were also added for this design. The pattern that is seen in Fig 23 is the pattern used in the final design. Notice that some folds do not have channels. Adding a channel to these folds would only add a ring to the tube without any purpose, meaning that the expansion rate would suffer.

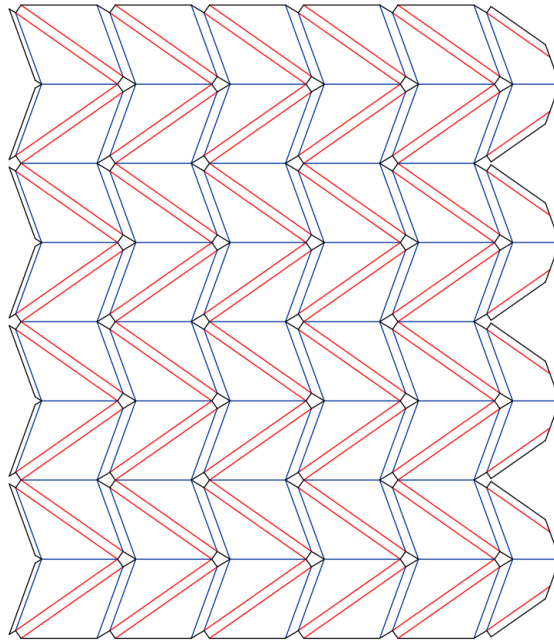


Figure 23: Folding pattern of the AXM module. RED=Valley fold, BLUE=Mountain fold, BLACK=cut

5.4 Fabrication method

Determining the material and production method go hand in hand. In this subsection, the focus will be on the production process explored and the material possibilities that came with it. At its basis, every module requires three types of parts: hinges, magnets and panels. For the magnets, small cylindrical neodymium magnets were bought and attached to or inserted into the panels. The production of the hinges and the panels was less straightforward, and thus three methods were explored and prototyped: 3D printing, Mould with resin, and Mould with sheet.

5.4.1 3D printing

3D printing was considered a valuable production method because a 3D printer can create and combine all panels and hinges into a single solid piece using living hinges. This could also enable the production process to operate on a much smaller scale, as only a higher-grade 3D printer would be necessary. But, even though 3D printers can operate at nanoscale, the printers most accessible during this thesis were Ultimakers and the Bambu Lab A1 mini with a nozzle of 0.4 mm, which makes the minimum line width approximately 0.24 mm [48] [66] [6] [4], which was verified during the production tests of this thesis. This meant that to print the desired living hinges, the tessellation needed to be scaled up. Requiring every tile of the waterbomb to be 5cm by 5 cm. This method would ultimately result in a giant prototype, but still, several tessellations with different living hinges were still produced. The hinges of the prototype tiles felt stiff and brittle. With signs of material fatigue already visible after opening and closing the prototype a few times. Even though with a different material and a higher quality printer, this method of production could still be viable, it was decided in the interest of time to explore other production techniques.

5.4.2 Mould with resin

The mould with resin production process used rigid panels, which were held in place by a mould; then a flexible resin was poured into the mould. When the resin has dried and the prototype has been removed from the mould, the prototype device is ready. To get a feel for the process, the production method was tested out to produce a single waterbomb tile, using 3d printed parts and hot glue. The mould, ejector and prototype that were made can be seen in Fig 24. Although the joints were much too stiff it showed the potential of this production process. There are many different types of epoxy; however, finding one that adheres to the panels and is flexible enough proved to be difficult. In the interest of time, this method was set in the background as well.

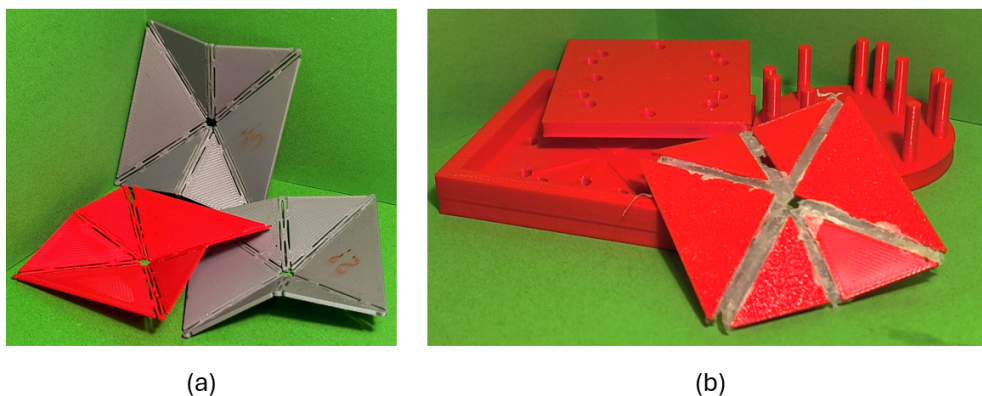


Figure 24: (a) 3D-printed prototypes of the waterbomb tessellation using living hinges. (b) Mould, ejector, and prototype that was made during this thesis.

5.4.3 Mould with sheet

The mould with sheet production process also uses rigid panels being held in place by a mould. However instead of pouring resin as with the mould with resin process, the panels are coated with a bit of glue on

the exposed side. Then, a sheet of flexible material is placed on top of these panels. For this thesis, the panels were 3D printed as this allowed for more control on the thickness of these panels. The sheet would ideally be made out of a biocompatible soft plastic. Polypropylene (PP) or Polyethylene (PE), then come to mind. However, due to its low energy and difficult-to-penetrate surface, glues have difficulty bonding to these two materials [17] [14] [12]. As no glue in non-specialised hardware stores could provide glue which stuck properly to the PP or PE, a different solution needed to be found. A method considered was using clear packing tape. These tapes are made of PP and already come with glue. However, prototyping the waterbomb pattern showed that this glue did not attach well to the panels. This can be seen in the bottom right of Fig 25. The panels displace when the pattern is folded even when both sides are taped.

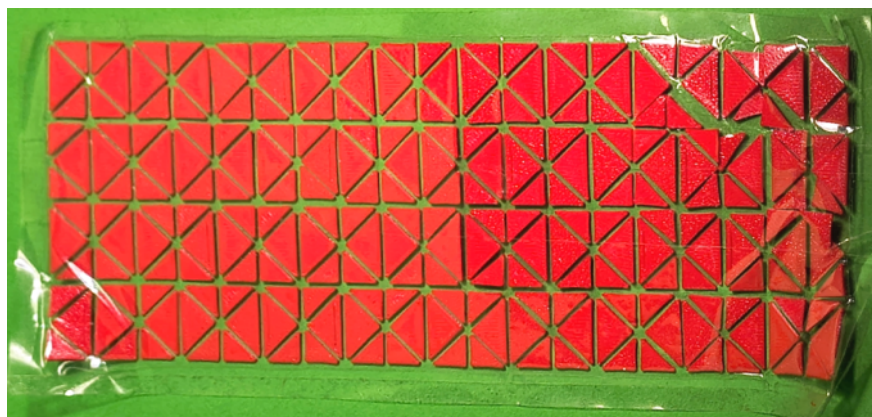


Figure 25: Unfolded waterbomb prototype, made by using clear packaging tape and PLA panels.

PEEK was also considered. However, the goal of this prototype is to determine whether these origami structures interacting with each other could lead to locomotion. So, biocompatibility is not yet necessary. Thus instead of investing in a PEEK sheet, the much more available paper was used.

Standard paper is stiffer than initially desired, and thus two methods of reducing this stiffness were identified. The first is using thinner paper. To test the effectiveness of this approach, three different thicknesses of paper were used: standard A4 printer paper, which is 80 grams per square meter (gsm), thin printer paper of 50 gsm, transparent paper of 42 gsm, and 200H carbon paper with a weight of 28 gsm. During testing, the thin paper and printer paper were able to maintain their structural integrity; however, the transparent paper and carbon paper had insufficient stiffness to counteract the magnetic attraction between the magnets and would collapse once the panels and magnets were in place. For all papers and panels, "Loctide Super Glue-3" worked without any problems in attaching the PLA panels to the paper.

The other method of reducing the stiffness of the paper was to reduce the thickness of the paper only at the hinges. By engraving the joints using a laser cutter, paper is removed at the desired locations. To engrave paper, the laser cutter must engrave at the perfect speed and with laser power. If the speed is too low or the laser too intense, a cut is created; if the speed is too high or the laser intensity is too low, the engraving is not significant enough.

So for both 80 gsm and 50 gsm paper, an experiment was conducted to find the ideal combination of speed and power. This was done by asking the laser cutter to cut a line at different intensities and power. The test setup can be found in Appendix 11.2. The lines were judged on how well they were engraved on the paper. A scan of all lines can be found in Appendix 11.3. The resulting grades can be found in Appendix 11.3.3.

From these experiments came several settings that could be used. Such as a power percentage of 6 and speed of 5 for both paper thicknesses. However, the most interesting thing was the unintended result of perforation. This happens because the laser blinks at a constant frequency; if the speed is high enough, the location of the blink is always at a different location. And if the laser is powerful enough to perforate the paper during one such blink, a perforation is created.

This perforation method is, relative to engraving, more reliable as paper is difficult lay down flat and is also quicker. Increasing or decreasing flexibility is also easier, as doubling the speed cuts the number

of perforations in half. Therefore, perforation was chosen as the method to introduce flexibility into the paper. The perforation, however, made the prototypes more fragile; the 50 gsm paper was difficult to assemble without tearing, so 80 gsm paper was chosen as the final material. After informal testing, the best perforation was seen with a power percentage of 17 % and speed of 10. Cutting was done with the same power, just at a speed of 2.5.

After perforation, the laser-cutter cut the outside lines of the pattern. On the resulting sheet, the panels were manually glued at the desired location using a stencil. The required panels had holes that allowed the magnets to be positioned correctly. A picture of this process can be seen in Fig 26. After that, when the glue dried, the RM module was folded into its desired shape.

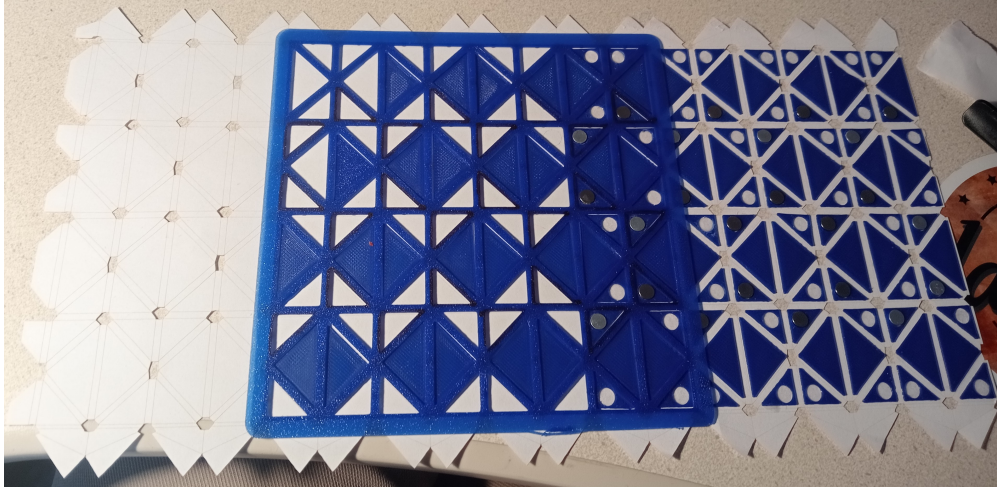


Figure 26: Assembly of an RM prototype, using a stencil to place the panels at the desired location

In conclusion, after careful consideration, the best production method to create the prototypes is to first perforate the hinges onto standard 80 gsm paper using a laser cutter, after which the outside lines are cut. Then, using Loctide Super glue-3, the PLA 3D-printed panels are glued on top of the paper using a stencil. After that the magnets are placed in the correct orientation inside the holes of the panels. The entire system is manually folded and glued into a tube, resulting in the finished prototype.

5.5 Magnet placement

Before determining the magnet placement of a specific origami pattern it is important to consider the relationship between the number of possible magnets and the spring stiffness of the joints. If magnets are placed close to each other, they will attract each other. The spring stiffness of the joints normally prevents this from happening. However, if, during any folding configuration, the magnets get too close to each other, it will lead to a collapse. Thus, one could argue that as few magnets as possible should be used. However, reducing the number of magnets reduces the expansion rate and speed, which are desired properties for the prototype. Thus, as many magnets as possible need to be placed without the magnets attracting each other with a force higher than that created by the spring stiffness of the joints.

5.5.1 Magnet placement for RM-module

To determine the optimal magnet placement, it is first necessary to consider the ideal magnet placement scenario, assuming no repercussions from placing too many magnets. Additionally, it was assumed that every panel could be transformed into a dipole magnet in any direction. To maintain radial symmetry, every tile of the RM would have the same magnet setup; this simplifies the search for the optimal setup, as only one tile needs to be considered.

In previous research, a Matlab model was used to simulate the behaviour of origami structures with magnetic panels inside uniform magnetic fields [60]. This model has a downside in that it can only model

small-scale structures such as single or double tessellations. However, as only one tessellation needs to be simulated for this experiment, this script was used to find the optimal magnet placements.

The important inputs of the model are as follows: Origami pattern, initial displacement, magnetic strength vector of each panel, magnetic field vector of the uniform magnetic field, DOF for every node, and spring stiffness of the joints. The output is the angle relative to the magnetic field of all panels when the spring stiffness and the magnetic torque are in equilibrium.

Using this script, the optimal magnet direction was decided. Four magnet tessellation configurations were run through the model. All configurations had to retract as much as possible from an already slightly contracted position. The only difference between configurations is the direction of the magnetic field vector of the panels. The top panels of Fig. 27 show the magnetic field vector direction of the panels, with + meaning the magnetic vector is facing towards the reader - means the magnetic vector is facing away from the reader, O means the panel has no magnetic properties, and an arrow shows the magnetic field vector orientation if the field is aligned with the paper. Lastly, the Ba arrow represents the direction of the magnetic field. The plots below these configuration panels shows the resulting displacement when applying that specific configuration.

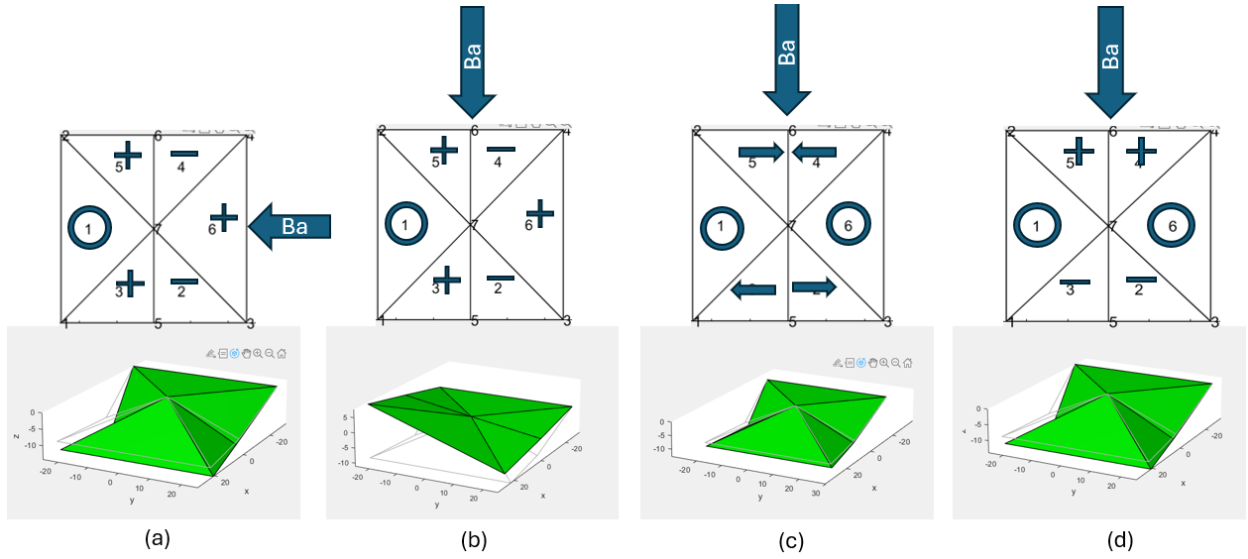


Figure 27: Magnet placement for the RM and its resulting simulated behaviour for configuration a,b,c, and d.

To determine how much the structure has retracted, the angle between panels 1 and 6 is used as a parameter. As panel 1 is locked at 0 degrees, which can be seen in Fig 27e, the angle between panel 1 and 6 will be referred to as the retraction index and can be calculated as follows: $180 - \text{angle panel six} = \text{retraction index}$. Therefore, a smaller retraction index means more retraction.

Configuration (a) -The first configuration tested on its retraction index was configuration (a) as a baseline test. This configuration of the waterbomb came with the script and is shown in Fig. 27a, where it was proven to work. This configuration was also used to determine the initial inputs, such as stiffness and magnetic strength. This resulted in a retraction index of 145.2° .

Configuration (b) -A problem with configuration (a) is, however, that the magnetic field comes from the wrong direction, the magnetic field of configuration a is not in line with the symmetry axis of the tessellation. Thus, configuration (b), which can be seen in Fig 27b, changes nothing else but aligns the magnetic field along the symmetry axis. Which results in the tile not folding properly and thus has no proper retraction index.

Configuration (c) -The following configuration was 'Configuration c'. Instead of pointing out of the paper, the magnets are placed in line with the paper, and the magnet on panel 6 is removed, see Fig 27c. This leads to a retraction index of 167.25° .

Configuration (d) -The last configuration can be seen in Fig 27d, here the magnets are pointing out the paper. Which leads to an even better result with a retraction index of 166.07° . This result can be seen in Fig 27h.

Table 4: Retraction index of the different magnet placement configurations for the RM module

Configuration	Retraction index
(a)	145.2
(b)	-
(c)	167.2
(d)	166.07

All retraction indexes are summarised in Tab 4. Configuration (a) has the best retraction index, as it has an extra magnet on panel 6. However, the magnetic field being in the wrong direction means that this configuration can not be used. Second comes configuration (d), which is the configuration that will be used for the prototype. Configuration (c) & (d) receive the exact same forces but inversed. If the focus is on retraction, then 3 is ideal, while if the focus is on extension, then 4 is more ideal.

Reality is, however, that placing a magnet on all tiles, as implied by these tests, will result in the magnets stacking onto each other. After testing out different layouts, a layout was found that the RM module allowed 50 % of the desired planes to have a magnet. See Fig 28 the outer planes do not have a magnet as these planes are static. This configuration makes sure that when collapsed always, four planes are between every magnet; this ensures that the magnets stay at a distance from each other and thus have a low magnetic attraction to one another. This layout also does not reduce the axial symmetry.

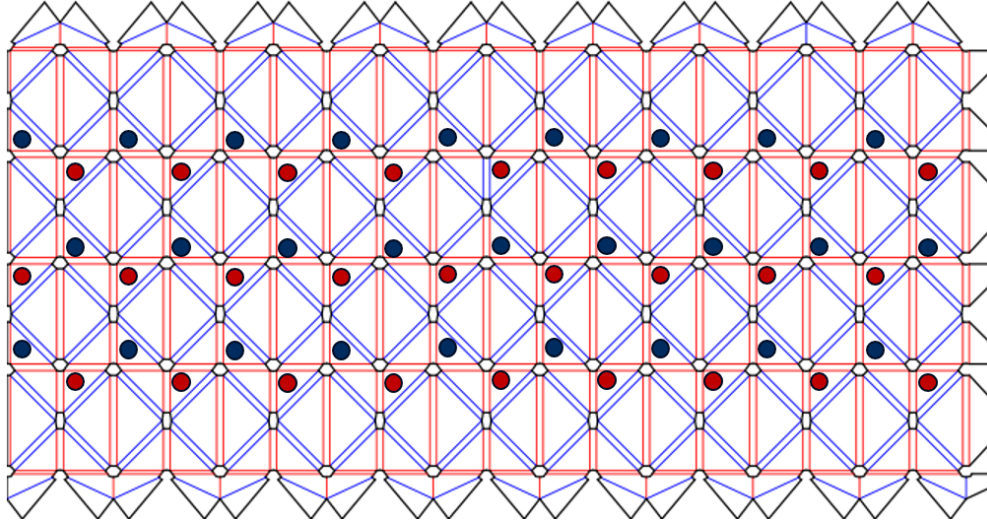


Figure 28: Crease pattern of the RM with magnets, red dots mean the magnet is facing towards the reader, blue dot means the magnet is facing away from the reader.

5.5.2 Magnet placement for AXM-module

Deciding the ideal magnetic placement of the magnetic direction for the AXM was more straightforward. Two configurations were tested, with the difference being that the first configuration has the magnets pointing out of the paper while the second has the magnets in line with the paper. The schematics of these configurations can be seen in Fig 29a and 29b.

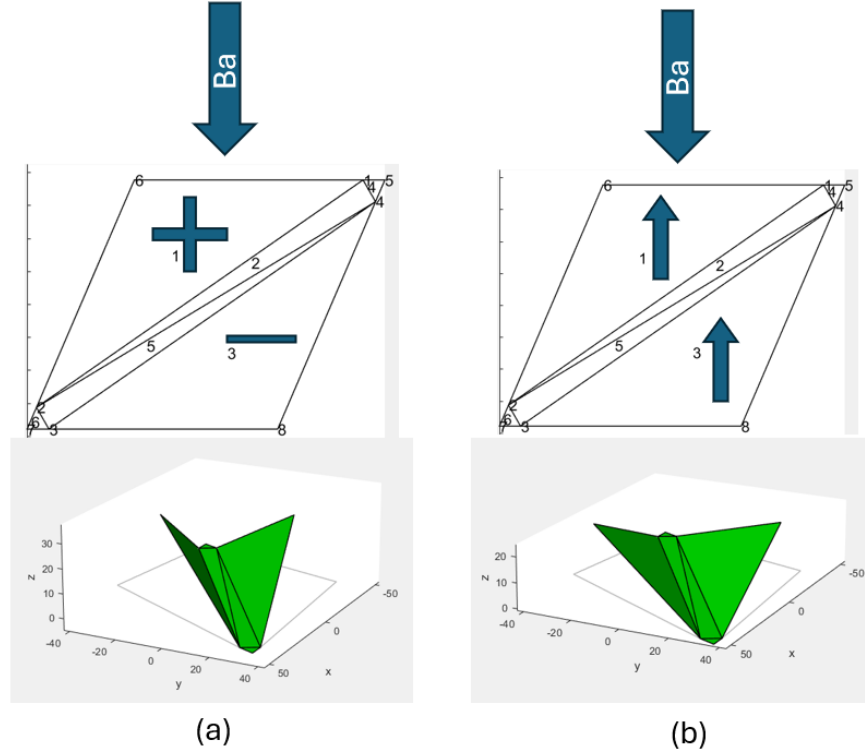


Figure 29: Magnet placement for the AXM and its resulting simulated behaviour

Table 5: Retraction index of the different magnet placement configurations for the AXM module

Configuration	Retraction index
(a)	68
(b)	105

All nodes except for 6 and 8 are locked, meaning only panels 1 and 3 can move. The retraction index is calculated as the angle between panels 1 and 3 at the equilibrium of forces, just like with the RM simulations. The retraction index can be found in Table 29, where, once again, a lower value is a better retraction. Both in Table 5 as visually in Fig 29, it can be seen that 'Configuration a' collapses more than 'Configuration b'. And as this setup is also easier to prototype, it was decided to proceed with this magnet placement.

Just as with the RM magnet placement, for the AXM module it is important that the magnets are not too close to each other, in Fig 30a a prototype can be seen where 50 % of the desired panels had magnets. This results, however, in a total collapse of the origami as all magnets attracted each other. During the production of the RM prototype, it was found that 4 segments between each magnet prevented this collapse. Applying that to the AXM resulted in 25 % of the panels that could have a magnet having a magnet. This is the maximum number of magnets that can be fitted while maintaining the axial symmetry and was thus used in the prototype. The crease pattern with magnet placement can be found in Fig 30b.

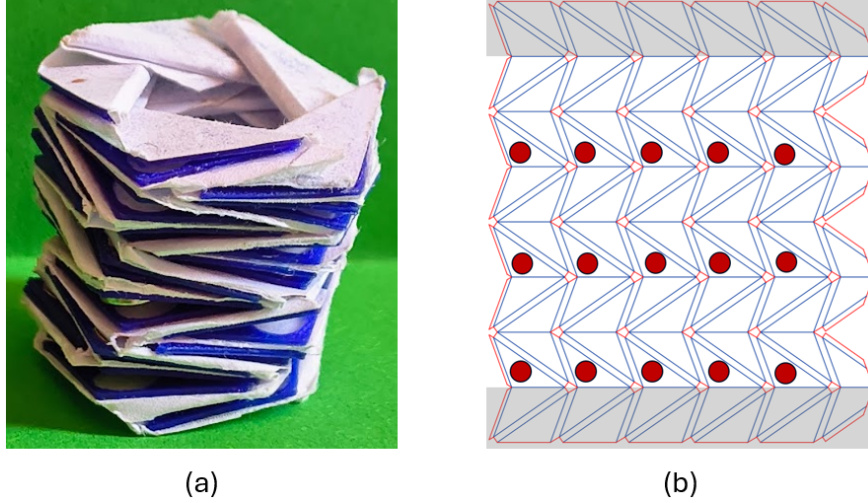


Figure 30: (a) Picture of AXM with too many magnets, which results in a permanent state of collapse. (b) The crease pattern of the working AXM, with magnets (red dots) and panels. Panels in the grey zone are used for the interface between the RM and AXM and are static.

5.6 Integration

The final step in the production of the prototype is to combine the modules together. The AXM is the centrepiece and already has a static plane at both ends of its tube. The RM1 also has static panels on both ends. Using a bit of additional paper and glue, as can be seen in Fig 31, the two modules can be connected. RM2 is identical to RM1, just rotated 180° and can be connected similarly.

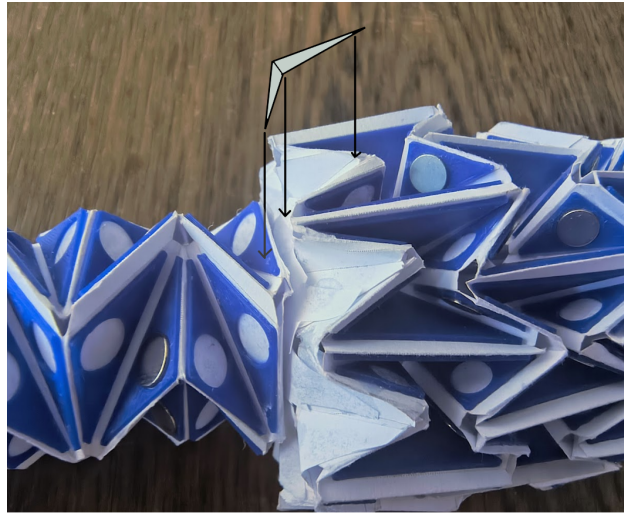


Figure 31: Picture of the integrated modules with a sketch of the integration piece

5.7 Conclusion of final design

Based on the final concept the final design was fully defined. Different locomotion sequences were identified but a 1 DOF sequence that uses a delay between the AXM and RM in expansion was chosen as the locomotion method. To facilitate this locomotion method additional requirements were made for each module. These requirements were then used to find the ideal origami pattern, material, magnet placement, and production process for the prototype. The waterbomb tessellation was deemed the most optimal for the RM, while the

"Collapsible Tower Dodecagon V2 With Sectioned Folds" without sectioned folds seemed as the base usage for the AXM. For both these origami patterns channels needed to be added on the location of the folds to allow the thick-panelled origami to fold. The orientation of the magnets on the origami was determined by using a model of a single tile of the origami pattern. The production process consisted of glueing PLA panels on top of A4 paper, in which folding lines were perforated using a laser cutter. After which, magnets were placed in such a way as to have as many magnets as possible without them attracting each other. The final step was attaching the interfaces of the modules together to form one prototype.

6 Module experiments

To determine if the modules would work as theorised, two sets of experiments were done on the separate modules. The first set explores the behaviour of the modules separately in a quasi-static magnetic field to provide insight into the folding behaviour, the expansion, and the potential history being present. The second experiment tests the module's step response using a square wave as input for the magnetic field. This is done to collect the prototype's expansion speed and further gain insight into the behaviour of the module. At the end of every experiment, the results will immediately be shown and discussed.

6.1 Setup

The test setup can be seen in Fig 32. Its basis is the PACMAG, which, using only its X-axis coils, creates a magnetic field. The maximum field strength that can be generated is 50 mT in two directions, so the range of the magnetic field is 50 to -50 mT. Inside this magnetic field, the module is placed along a glass rod. A camera from above captured a frame every 500 ms for 10 cycles. The resulting video was then used to track the radial expansion of the RM. The axial expansion was tracked for the AXM. The software used to track this was "Tracker - Video Analysis and Modeling Tool" [13].

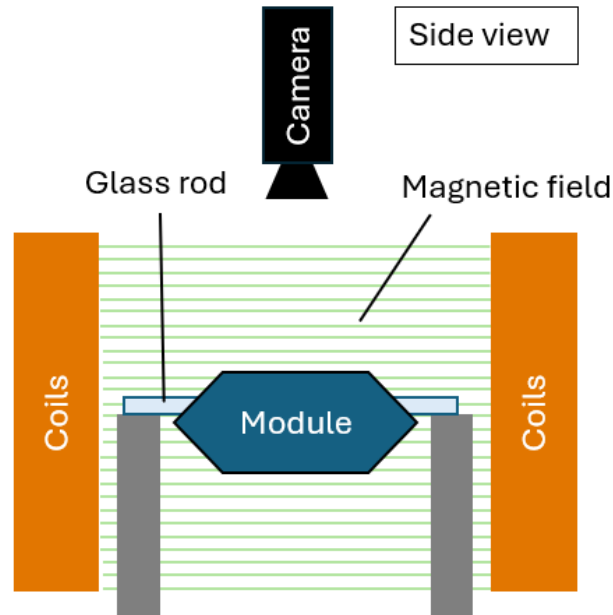


Figure 32: Sketch of setup used during the separate modules experiments

6.2 Quasi-static input

As mentioned in the intro, the goal of this experiment is to gain insight into the folding behaviour of the modules and know the expansion rate. As input, a slowly rising magnetic field was used. This field slowly alternated between 50 mT and -50 mT in a sinuswave with a cycle time of 20 s. Such a long cycle means that inertia is negligible in the results, thus the input is quasi-static. All behaviour is purely a result of the geometry of the origami and its interaction with the magnets.

Table 6: Results of the quasi-static input experiments

	RM (diameter)	AXM (length)
Collapsed size (mm)	59.0	56.3
Expanded size (mm)	69.8	68.0
Expansion rate	18%	21%

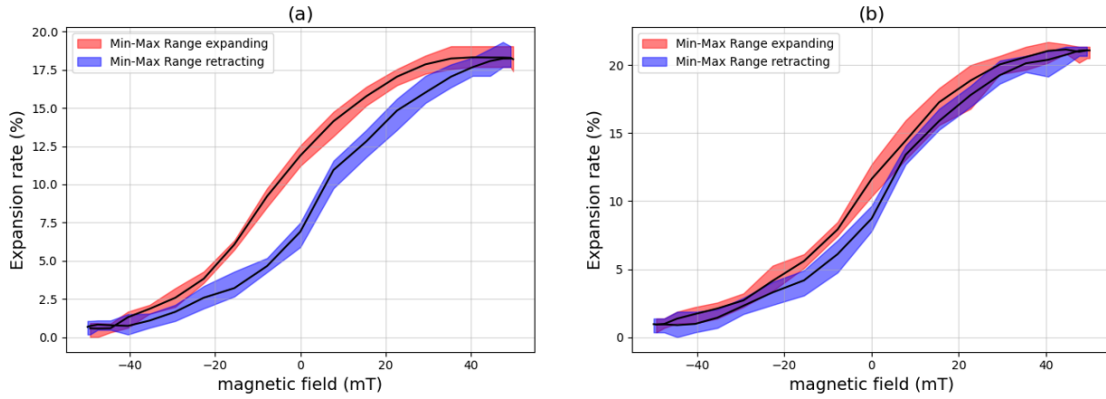


Figure 33: Results of the quasi-static field experiment for a) the RM module and b) the AXM module.

The resulting expansion of both the RM and the AXM can be found in Table 6 and Fig 33. The graph illustrates the expansion rate of the module in response to the magnetic field. It consists of two parts: red, which shows the expansion rate for different magnetic fields when the waterbomb is expanding. And blue, showing the expansion rate at different magnetic fields when the waterbomb is retracting. The black line represents the mean, while the coloured area indicates the range between the magnetic field's maximum and minimum expansion rates. Snapshots of the experiment can be found in Fig 34 and Fig 35

The first thing to notice is the S-shape of all the curves; this indicates that the displacement created by increasing from 0 to 10 mT is greater than that created by increasing from 40 to 50. This makes sense as the spring stiffness increases linearly while the magnetic torque increases along a sinewave (see Appendix 11.4 Modeling). The second thing to notice in the graph of Fig 33 is that especially the RM seems to have the behaviour that it matters whether or not the module was just expanded or retracted. For example, the expansion rate when the field is off (so 0 mT) is 12 % when coming from a total retraction, while the expansion rate is 7 % when coming from total expansion. This is counterintuitive, as a baseline resistance would explain the opposite behaviour. The reason remains unknown. The most important data from both the graphs and the table is that the maximum expansion rate of the prototype can be read. For the RM, the expansion rate is 18 %, whereas for the AXM, the expansion rate is 21 %.

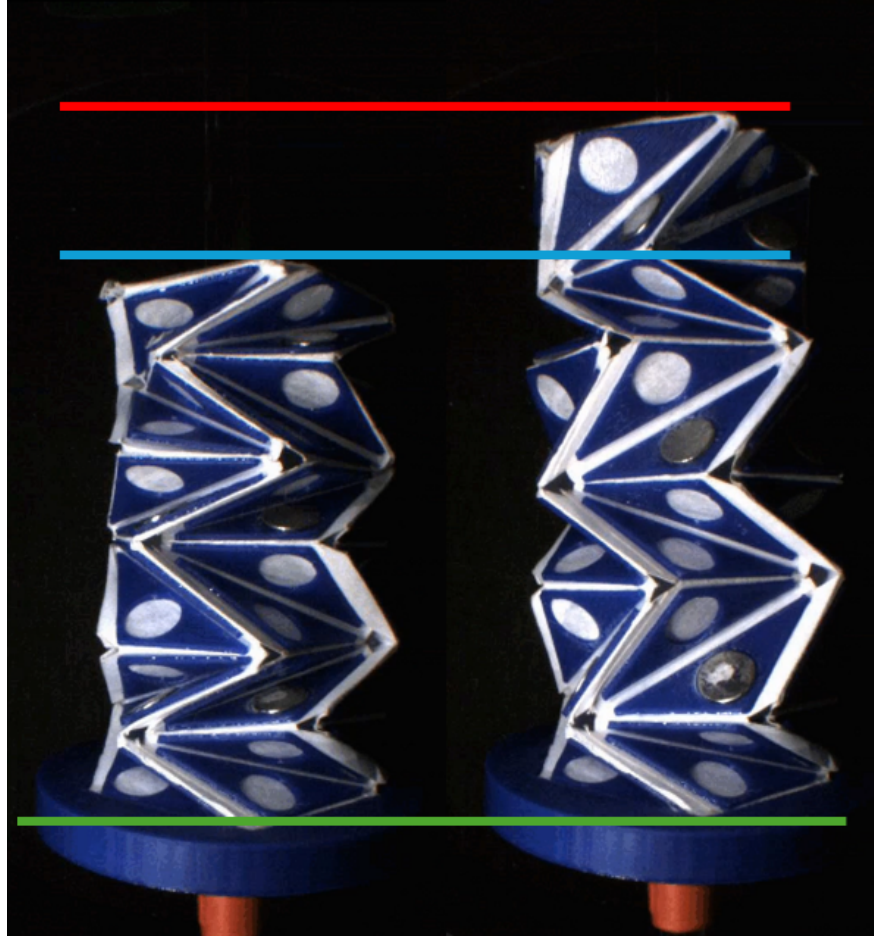


Figure 34: Frames of AXM module being both collapsed and expanded during the quasi-static input experiment. Green: Baseline, Blue: maximum retraction, Red: maximum expansion



Figure 35: Frames of RM module being both collapsed and expanded during the quasi-static input experiment. Green: Baseline, Blue: maximum retraction, Red: maximum expansion

6.3 Square wave input

The following experiment had the goal to determine the expansion speed of the modules and gain more insight into the behaviour of the modules.

For this test, the same setup was used as with the quasi-static experiment. The only two changes are that the magnetic field now instantly switches from -50 mT to 50 mT and vice versa every second. The other change is that the camera now captures at every 0.022 ms, better known as 45 frames per second. The settling time was determined by measuring when the average of all cycles reached 95 % expansion. Retracting time was determined by the time it takes the average to reach 5 %. As the system has to stabilise, the latest point that the 95 % or 5 % line is crossed is measured.

Table 7: Settling times of RM and AXM.

Module	Time to 95% (ms)	Time to 5% (ms)
RM	505	420
AXM	201	195
Δ	304	225

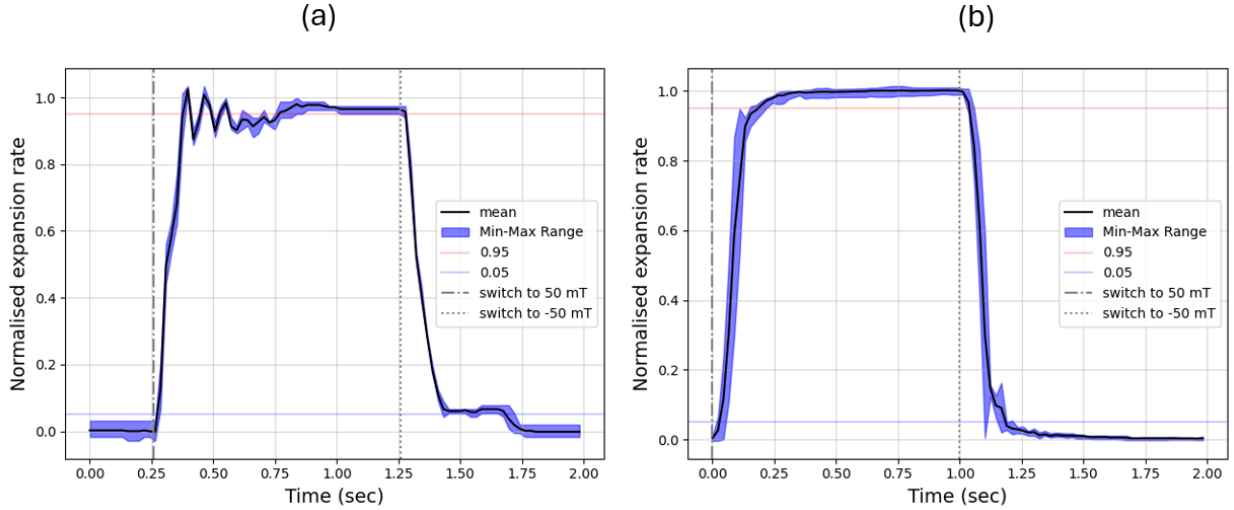


Figure 36: Average normalised expansion rate over four cycles for (a): the RM. And (b) the AXM

The graphs of the RM and AXM can be found in Fig 36a & b, respectively. The time it takes for the modules to reach the 95 % and 5 % mark can be found in Table 7. The results of the AXM give a good insight into the behaviour of this module. However, the expansion and retraction time is a bit lower than that of the RM. In reality, the AXM module will take longer as it needs to displace the RM, thus having more momentum.

Based on these results, a model was developed to predict the expansion rate if certain parameters were changed. This model was based on an MSD model, as during the production of the modules, the modules seemed to behave in a similar way. However, the model could not be verified during this thesis and needs to be heavily adjusted with the data of the integration test. For these two reasons, it was decided not to use the model or its predicted values. The model can be found in Appendix 11.4.

6.4 Conclusion of module experiments

In this chapter, the modules were tested separately inside both a quasi static field and a quickly changing square wave field. The quasi-static experiments showed that the RM and AXM expanded 18 and 21 percent, respectively, which is below the 20 and 100 percent goal set in the requirements. It also showed that the

expansion rate at a certain value is dependent on whether the module was previously expanded or collapsed. The reason for this, however, is unknown. The square wave input gave insight into the responsive behaviour of the modules. Showing that the RM needs about half a second to fully react to the change in the field. The AXM reaction time was also used. But its reaction time is most likely much larger in reality as then it has much more mass to push. Based on these experiments, a model was developed to predict how adjusting parameters would change the behaviour of the modules. This model was based on an MSD model but was scrapped as the model could not be verified during the thesis and had to be adjusted heavily after the integration experiments.

7 Integration experiment

An integration test was done to determine whether the modules behaved as expected as a system. A prototype was made by glueing and fixing the separate modules together. The prototype was placed inside a tube inside an alternating uniform magnetic field along the symmetry axis, as described in chapter 5.1 Locomotion. The speed of the prototype at different cycle lengths was measured to determine the optimal frequency to switch the magnetic field. Also, the expansion of the separate modules was measured to verify the prototype locomotes as expected. Due to the performance of the individual modules in the previous experiments, the expectation was that the prototype would not move forward.

7.1 Setup

The 3 modules were connected using glue and additional paper to increase the glue area. Note that RM2 is identical to RM1 but is rotated 180° . The system was placed inside a PVC tube with an inside diameter of 63 mm. Which in turn was placed inside the Helmholtz coil setup named PACMAG. The diameter of 63 mm was chosen as this was the largest diameter possible to fit inside PACMAG, and a smaller diameter would result in too much friction. To reduce friction even more, acryl-glass sanding dust was sprinkled along the inside of the tube. A setup sketch can be found in Fig 37. The PACMAG was instructed to switch between 40 and -40 mT. 50 mT was tried; however, it resulted in the disconnect of magnets from the prototype.

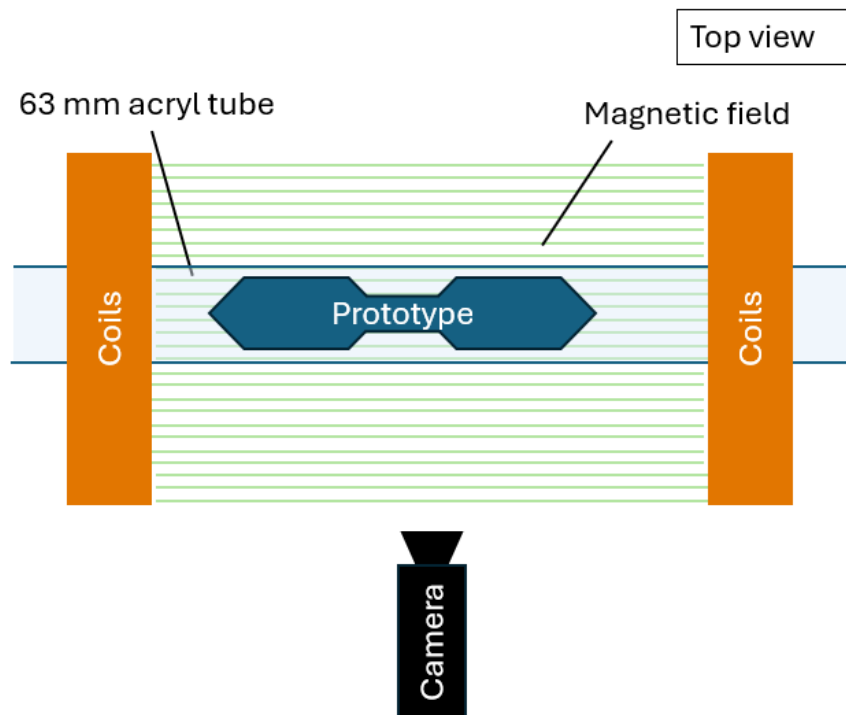


Figure 37: Sketch of setup used during the integration experiments.

7.2 Results of integration experiments

Table 8: Absolute results of integration experiments showing expansion of the modules

Cycle length (s)	RM min/max (mm)	RM expansion	AXM min/max D (mm)	AXM expansion
0.01	47/50	6%	69/71	3%
0.1	46/53	14%	69/72	4%
0.19	46/55	21%	68/73	7%
0.25	48/57	19%	68/72	5%
0.5	45/58	29%	64/75	18%
1	42/54	29%	64/72	11%
2	43/56	32%	63/72	15%
3	42/55	30%	64/75	18%
4	45/56	26%	67/75	11%

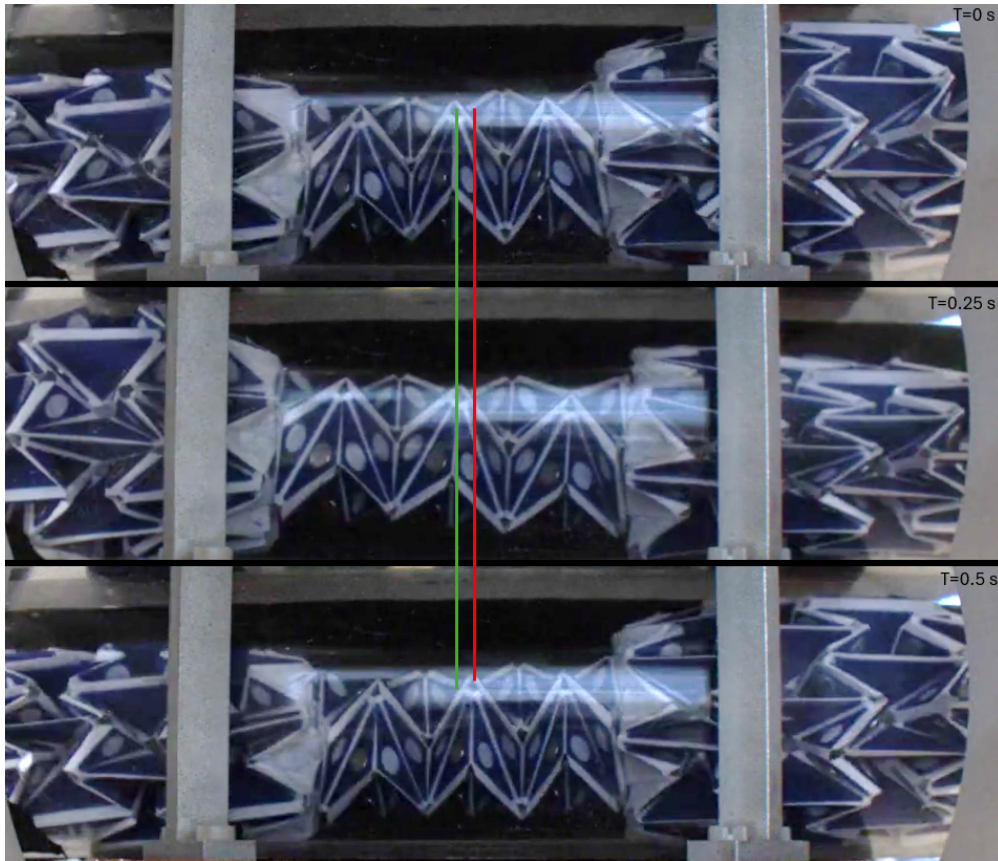


Figure 38: Three snapshots of the prototype during the experiment with a cycle length of 0.5 seconds. Displacement over one cycle is displayed with the green and red lines.

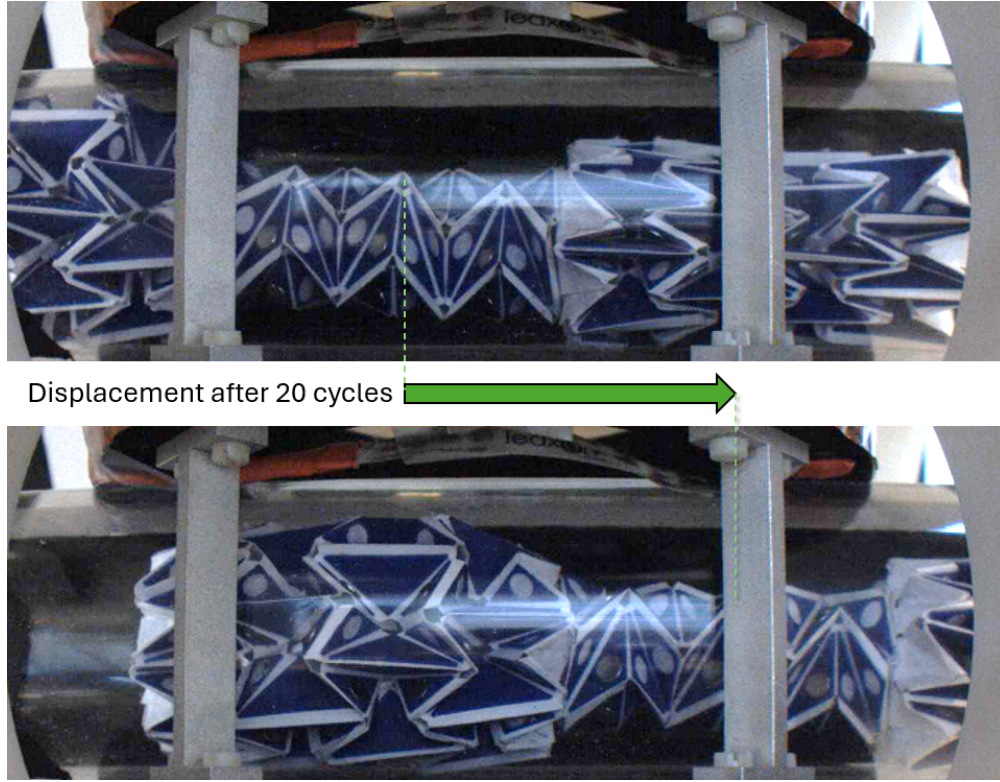


Figure 39: Displacement of prototype after 20 cycles of 0.5 s PD

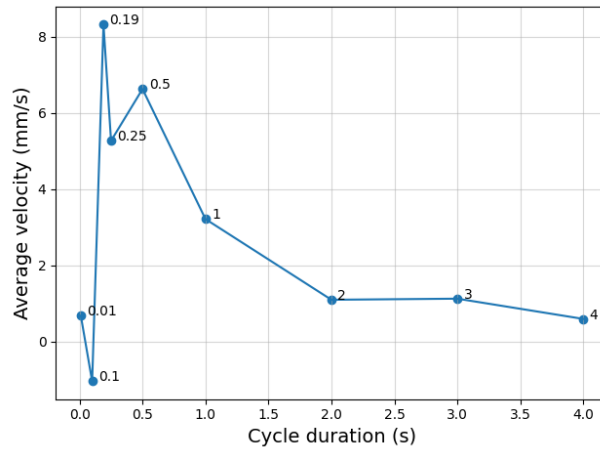


Figure 40: Plot of the average velocity as a result of different PDs.

The prototype moved forward during the experiments. The velocities vary depending on cycle length; these results can be seen in Fig 38 and Fig 39. That the prototype moved forward was against the expectation as the RM module did not expand enough during the individual experiments to properly clamb. Additionally, it was unknown what the addition of displacing the RMs would have on the speed of the AXM. Nonetheless, the behaviour of the modules was analysed to explain the behaviour. The expansion rate of the separate modules during the integration experiments can be found in Table 8. The table contains a lot of information, but the most interesting behaviour is the expansion of the RM. That, when given enough time, expands to approximately 29 %. This is much higher than the 18 % during the separate module testing in section 6.2.

This is even more impressive considering the separate modular experiments were done up to 50 mT, while the separate integration experiment used only a magnetic field of 40 mT. The absolute expansion values are closer, with the separate RM module expanding 11 mm, and the integrated RM module expanding between 9 and 13 mm. The reason the expansion rate in percentages differs so much between the separate and integrated experiments is that the minimum radius is much smaller for the integrated RM than that of the separate RM (59 mm against around 43 mm). The current understanding is that this difference is due to the prototype hanging along a glass rod during the separate module test, where gravity causes the hanging modules to be larger when no field is applied relative to the modules when it is lying at the bottom of the tube and gravity pushes it inwards. But for both cases, when a field is applied, the same absolute displacement happens, and as the hanging module baseline is larger, the expansion rate in percentages is less.

7.3 Optimising phase duration

The phase duration (PD) (previously mentioned as cycle length) is the time between every two alternations. It is still unknown what the optimal PD is for the prototype to locomote optimally. To investigate this, different PDs were tested between 0.01 and 4 seconds. The middle of the axial module was used as a tracking point. The exact movement graph of every PD can be found in Appendix 11.6. The average speed of this point with every PD was then calculated. This resulted in the data seen that is visualised in Fig 40.

Analysis of the velocities reveals an interesting observation. The velocity at the PD of 4 seconds is 0.60 mm/s. Halving the PD should result in a doubling of the prototype's speed. However, halving the PD from 2 s to 1 s does not result in a velocity of 2.2 mm/s but 3.21 mm/s. An explanation can be that cycle times 4 and 2 must have a velocity of 0.75 and 1.5, respectively. This would make the data better fit the 1 and 3 seconds PD. The average speed is over multiple cycles, but as all tests were only done once, the possibility of this inaccuracy can not be rejected.

Leaving the larger PDs for now, the smaller PDs seem almost chaotic. The first reduction in speed (from PD of 0.5 to 0.25 s) can be logically explained as during the step input experiments the RM needed 0.5 seconds to stabilise. The magnetic field switching earlier than that would result in an imperfect grip and, thus, a lesser efficiency. However, this is in direct contrast with the next PD of 0.19 s, which results in the highest average velocity recorded in the experiment. Halving the PD once again then results in the prototype moving backwards. With the final PD of 0.01 seconds, leading to a small velocity forward. It might just be that the 0.19 s PD fits with a resonance frequency of the system, which causes the sudden increase in speed relative to the PD of 0.25. Due to its chaotic nature, it was decided that the prototype does not work reliably with the PDs of 0.25 s and lower. These results were thus ignored in future analysis.

7.4 Phase analysis

To investigate whether the prototype locomotes as theorised in chapter 5.1 Locomotion, the expansion of every module was tracked for several PDs. The expansions were normalised and plotted against time in the cycle and can be found in Fig 41.

The expectation was that the RM1 and RM2 alternate in expansion during one cycle, being completely out of phase. And that the AXM expansion has a small phase shift (in the form of a delay) relative to RM1. Where the more the AXM is out of phase with RM1, the more efficient the movement. Looking at the results of the experiments in the previously mentioned Fig 41 these expectations are mostly fulfilled. The RM1 and RM2 are completely out of phase. And the AXM is slightly out of phase with RM1. However, a PD of 0.1 has a negative velocity but the largest phase shift of AXM relative to RM1, but does not lead to proves that this device moves forward using the designed locomotion method.

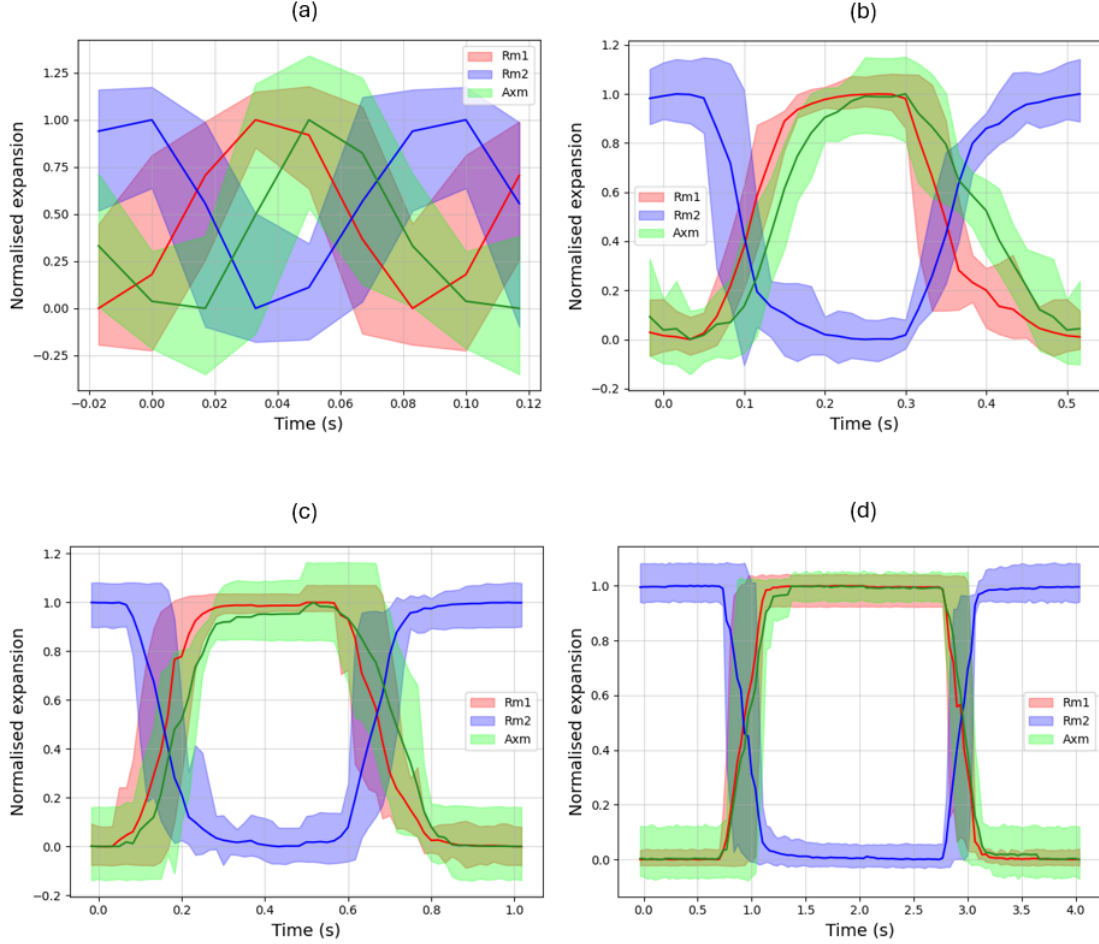


Figure 41: Plots of the expansion of each module when placed under differt phase times. a) PD=0.1 s, b) PD=0.5 s, c) PD=1 s, d) PD=4 s

7.5 Backwards motion

A drawback of this design that becomes increasingly more apparent is that this concept can not move backwards. This is because the RM1 and AXM open at the same time. Albeit with a small delay. It is important for the design to be able to move backwards, as otherwise, it is not possible to retrieve the device without additional surgery. Thus, the following requirement was added:

R10: The device must be able to reverse its direction.

The only method for the current prototype to go back along the path it came from is by making a U-turn. This is possible as the device aligns itself along the magnetic field at small changes in the magnetic field direction. To make such a U-turn, a large cavity is needed, and thus, only procedures such as through the Urethra to the bladder or from the mouth through the intestines to the anus would currently be possible. Endovascular purposes are more difficult as the system is much more compact, and large cavities for rotation are absent except for the heart.

Making the concept go backwards is possible in two ways. Either the AXM has to be in sync with RM2; in other words, change its phase 180° . Or the AXM needs to open just before RM1 instead of just after. Changing the phase of AXM such that it is in sync with RM2 is difficult. However, opening the AXM before RM1 is undoubtedly possible. Adding a Shape Memory Polymer (SMP) to critical hinges of RM1. The SMP

locks the angle of the hinges until electricity generated by an induction coil heats the SMP. This additional feature gives an additional degree of freedom to open and close the RM1 after AXM has been opened or closed.

7.6 Conclusion of integration experiment

To determine whether the modules would behave the same in an integrated system separately, an integration experiment was done. A prototype was made by connecting the two RMs to the AXM with glue and small pieces of paper. This prototype was placed inside an acrylic tube inside an oscillating uniform field. At PDs above 0.25 seconds, the prototype exhibited a steady upward movement as the AXM expanded more slowly than the RM modules. A PD of 0.5 s is the most optimal, which matches the expansion time of the RM during the separate module experiments.

8 Evaluation and discussion

In this chapter, the final design and prototype are weighed against the requirements set during the Preliminary design in chapter 4.1 and the additional requirements set in chapter 5.2. The evaluation is summarised in Table 9. The requirements are categorised into requirements that were met, requirements that were not met, and requirements that still need additional tests before a conclusion can be drawn.

Table 9: Evaluation of all requirements based on final prototype

	Requirement	Was requirement met?
R1	Outer diameter adaptability	Needs to be tested
R2	Aortic wall safety	Needs to be tested
R3	Locomotion	Yes
R4	Continued blood flow	Needs to be tested
R5	Failure rate	Needs to be tested
R6	Biocompatibility	No
R7	Simplicity	No
R8	Origami Engineering	Yes
R9	Magnetic Actuation	Yes
R10	Reversability	No
rm-R1	Radial expansion	Yes
rm-R2	No axial expansion	Yes
rm-R3	Module interface	Yes
rm-R4	Field along symmetry axis	Yes
rm-R5	Quick expansion	Yes
axm-R1	Axial expansion	Yes
axm-R2	No radial expansion	Yes
axm-R3	Module interface	Yes
axm-R4	Field along symmetry axis	Yes
axm-R5	Slow expansion	Yes

8.1 Requirements met

Locomotion (R3) - The integration experiments demonstrated that the current prototype is capable of displacing its centre of mass independently at speeds of up to 8 mm/s. This requirement has thus been met.

Origami Engineering (R8) - The device consists entirely of origami structures. Thus, the requirement to use origami engineering has been met.

Magnetic actuation (R9) - The device does move using a magnetic field, this requirement has been met.

Radial expansion (rm-R1) - The requirement set that the RM module should at least expand 19 %. During the individual modular tests, this expansion rate was only 18 %. However, during the integration test, expansion rates of up to 30 % were reached. The true value most likely lies between these two values. As explained in chapter 7.5 'Backwards motion', the reason for this difference is that even though they expand approximately 11 mm during both experiments. Gravity causes the hanging module during the separate experiment to have a larger base size relative to the integration experiment. The integration experiment has the prototype lying in a tube. Thus, gravity compresses the origami structure, resulting in a smaller base size. The final product will be much smaller and be submerged in liquid, reducing the influence of gravity. Thus, the expectation is that the true expansion rate lies somewhere in the middle of 18 % and 30 %. This means that this requirement has been fulfilled.

No axial expansion (rm-R2) - The origami design chosen for the waterbomb has no axial expansion. This requirement has been met.

Module interface (rm-R3) - The origami design chosen for the RM has a static interface that connects nicely to the AXM, as proven in the integration test. This requirement has been met.

Field along symmetry axis (rm-R4) - The origami design keeps the symmetry axis in line with the field. The magnet placement does not reduce the number of symmetry arms, so the number of symmetry arms is 9, which is a nice and high number. This requirement has been met.

Axial expansion (axm-R1) - The AXM has an axial expansion up to 18 %, although the initial goal of 100 % expansion was not met. The 18 % expansion is enough to allow locomotion. Although more cycles are needed for the displacement of the prototype. This requirement has been met.

8.2 Requirements not met

Biocompatibility (R6) - The materials chosen for the prototype were not selected for its biocompatibility. Printer paper, Loctite glue, and neodymium magnets are not biocompatible. Only PLA is, which even when 3D printed, can be biocompatible [24] [16]. Material is not the only factor determining biocompatibility; geometry, surface texture, and coating also need to be considered. This was, however, out of the scope of the project. So, to meet this requirement, the following needs to be done: Replace the paper and the glue with biocompatible alternatives and perform a biocompatibility study on the shape of this design.

Table 10: Number of parts used in the integration prototype

	AXM	RM1	RM2	Total per part
Magnets	15	54	54	123
Panels	80	216	216	512
Sheets of paper	1	1	1	3
Total per module	96	271	271	638

Simplicity (R7) - This requirement has not been met as the device consists of many components. The waterbomb pattern used has 36 tiles, with each tile having 6 plastic panels and 1.5 magnets; adding to that, the paper brings the total to 271 parts for only one RM. The AXM has a similar problem. The collapsable tower pattern used has 40 tiles, with each tile containing 2 plastic panels, with 15 magnets distributed over those panels. Once again, adding the piece of paper brings the total to 96 parts. The device consists, however, of two RM's and one AXM, which brings the final number of parts used to produce this device to 638. All of this is summarised in Table 10. 638 parts was deemed too high to call the device simple, so the requirement has not been met.

Reversability (R10) - As mentioned in chapter 7.5 'Backwards motion', the current prototype can not move backwards and reversing is only possible via a U-turn. This means that only procedures through a tube with an opening on both sides or towards a cavity are possible with the current device. Procedures going through the urethra to the bladder or through the intestine track are examples of such procedures. Endovascular procedures are much more difficult as there are no large cavities except the heart.

8.3 Requirements that need to be tested

Outer diameter adaptability (R1) This requirement consists of two parts. The first part is that the device needs to have a resting diameter of 31.44 mm. The outer diameter of the current design is determined by the diameter of the RM module, of which the resting diameter is around 51 mm (see Table 8). This means the current design needs to decrease in size by 38 % for this requirement to be met. The second part of the

requirement is that the prototype needs to be able to adjust its outer diameter with ± 8 %. This requirement was transformed using

$$\frac{1 + 0.08}{1 - 0.08} - 1 = \text{expansion rate} \quad (2)$$

to determine that the minimum expansion rate is 17 %. This is true for all experiments in Table 8 with a cycle length higher than 0.1 sec. Although these results give a good indication, this is no proof that the device can locomote through a tube with a varying diameter. As the locomotion method also uses the expansions of the RM, it might be that at the largest tube diameter, the prototype can not find enough traction or that at the smallest tube diameter, the traction is not decreased enough. If the device is further developed, it should be tested if the prototype can move forward in a tube with varying diameters.

Aortic Wall Safety (R2) - Although the design was made with aortic wall safety in mind, To test this requirement, the design must be set in stone, as material choice and a different expansion rate will be of great influence in keeping the aorta undamaged. The recommendation is thus to first optimise the design by defining the material and expansion rate, taking aortic wall safety in mind. Only after that can physical tests be started to determine the Aortic Wall Safety of the device.

Continued blood flow (R4) - Again, the device was designed to allow continued blood flow in mind. The device is hollow, and blood should be able to pass through it. However, this has not been tested virtually or practically during this thesis. As blood flow obstruction is defined by geometry, this can already be tested by virtually or physically measuring the pressure drop created by the prototype.

Failure rate (R5) - Although the current design has been made with minimal failure rate where possible. No quantifiable assessment has been made to determine whether this product is safe. But before that can be done, the design needs to be in further stages of the design process. With a set-in-stone design and a defined application for which the device will be used.

8.4 Conclusion of evaluation

Of the 10 main requirements, three were met, three requirements were not met, and five needed to be tested for it to be determined. The failed requirements were due to the prototype not being ready for the human body, as the prototype is not biocompatible, is overly complex and is not able to reverse its direction. The requirements that still need to be tested are in the outer diameter adaptability, whether the prototype is safe for the aortic wall, if it allows continued blood flow and the lack of a failure mode analysis. Most of these requirements that still need to be tested are dependent on the design being in its final iterative stages, with the correct material and circumstances. The 10 additional requirements, specifically for the separate modules, were all met, which is reflected in the fact that the prototype moves during the integration test.

9 Future research

As seen in the evaluation, the prototype still needs to be altered to fulfil all the requirements and become a functional product. In this chapter, first, what needs to be done to fulfil the requirements that were not met is discussed. Then, a possible future design is presented that applies these solutions. The chapter ends with potential uses for the soft robot, if it became a product.

9.1 Solving unmet requirements

The three requirements that were not met were Biocompatibility, Simplicity, and Reversability. In this subchapter, each is discussed as to what would need to happen to make the device fulfil those requirements. Aside from these 3 requirements there are 4 other requirements that have not been met as they are inconclusive, all need to be researched further, but will not be expanded upon in this subchapter.

To fulfil the biocompatibility requirement, materials need to be found to replace the paper, the glue, and the magnets. An alternative is to use a coating such as Teflon [33]. The surface texture of the materials is also an important factor in determining the biocompatibility of a part, this was out of the scope of the thesis and should be researched further.

With 638 parts, the design was not deemed to fulfil the requirement Simplicity. Reducing the number of parts is possible by integrating the plastic panels into the paper. For example, by using much thicker paper or other stiffer material and using a laser-cutter to remove material and keep the hinge stiffness the same. The number of parts are reduced from 638 to 126, which consists of 123 magnets and 3 laser-cut sheets. Additionally, reducing the number of magnets is possible by using a sheet of soft magnetic material instead of paper and once again using the laser-cutter to create the hinges such that the hinge stiffness remains the same. Using local magnetic fields, certain parts of the soft magnetic material can be magnetised. If both these steps could be achieved, the number of parts would be reduced to only 3. Testing this method of production fell outside the scope of this thesis and could be done in future research.

The current prototype is unable to move backwards, which makes retrieval of the device difficult. Adding backwards motion would involve letting the AXM open and close just before the RM1 instead of just after. To realise the relative phase change of AXM and RM1, an SMP can be placed on the critical hinges of RM1. This SMP locks the state of the RM1. However, by heating up the SMP using electrical current generated from induction coils, the SMP becomes soft, and the RM1 can change its state. This change makes it possible to open the RM1 after AXM has opened. Thus making it possible to change its direction. This method is similar to the locomotion method proposed in chapter 5.1 Locomotion, Figure 15c. The difference is that the AXM is locked via SMP instead of the RM1 in the earlier proposed method. For this other method to allow backwards motion, the AXM needs to be faster than the RM1, such that via the SMP, it can be decided to open the AXM before or after RM1. Currently, the AXM is not faster than the RM1; thus, the SMP is placed on RM1. However, this comes with the drawback that there might be a state at which both RM modules have limited grip on the aortic wall, which is undesirable. If it is decided to continue this research, it could be very interesting to further explore the use of SMP locked hinges on origami soft robots.

9.2 Future design

Using the improvement points of the requirements that were not met, a new design was sketched to illustrate what the final design could be. This sketch can be found in Fig 42. The design shares many similarities with the prototype in terms of shape, but that is where the similarities end. Instead of using separate panels, magnets, and paper, the design employs a different approach. The entire system consists of 3 laser-cut parts. Instead of separate magnets, the material will be infused with metal particles which are locally magnetised to the desired magnetic vector. To accommodate the device to move backwards, SMP is placed at the largest hinges of the RM1. Through the SMP runs a copper wire that can be heated up by creating a current using the induction coil. Only when a current is placed induced and the SMP is heated up can the RM1 change its state, this change is visualised in Fig 43. The size of the entire system would be smaller with 38 %.

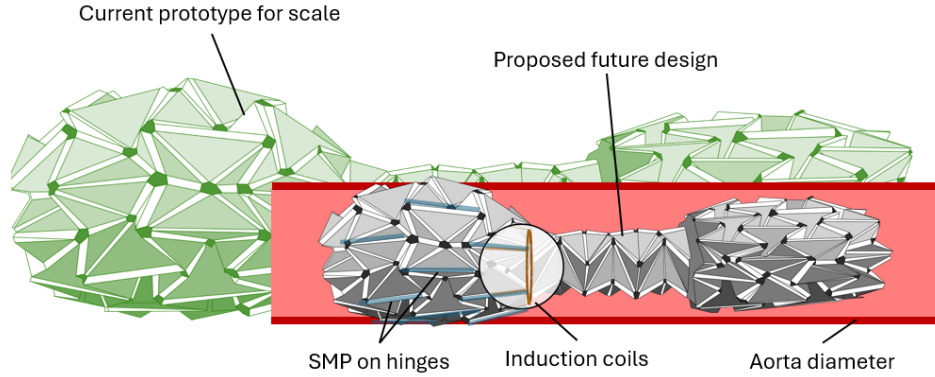


Figure 42: Sketch of the potential future design with induction coils.

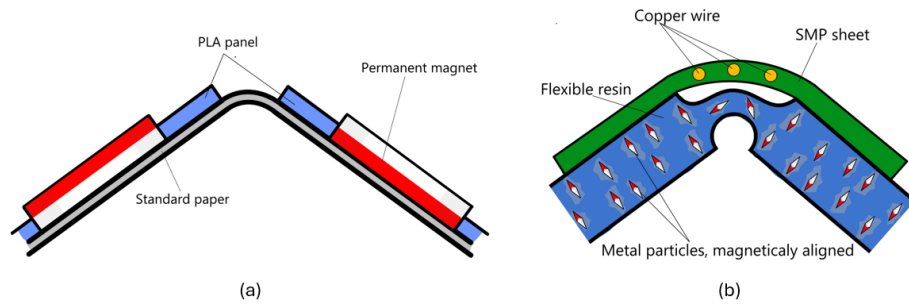


Figure 43: a) Sketch of the current hinge system. b) sketch of proposed hinge system for future research

9.3 Potential uses

The device was designed to aid stent placement in the aorta, and with more research, this goal is possible. However, there are also other use-case scenarios that this device might aid. There are four systems identified in which the device could be proven to provide useful aid: The circulatory system, the respiratory system, the digestive system, and the urinary system. These will be discussed one by one.

The circulatory system is a given, the device was created to aid in AAA and thus designed to traverse arteries. But scaling down the system even more would also allow the device to traverse smaller arteries or aid cardiovascular treatments. Robots to aid the movement of the guidewire are already in development, and this device could be a good alternative [39]. For aiding the respiratory system, the continued blood flow parameter really shines. The potential ability to traverse the windpipe without blocking air flow could be an interesting alternative to bronchoscopy. For the digestive system capsule robots are already in development, as mentioned in Chapter 3.7 'State of the art'. This device would distinguish itself from competitors as it can traverse the digestive tract without relying on the peristaltic movement of the bowels. With the addition the device does not need to move backwards, meaning no SMPs are needed. For the urinary tract, the device, if scaled down sufficiently, can be placed via the bladder inside the ureters or urethra to remove kidney stones that have become stuck and would otherwise require surgery.

It is tempting to scale up the size of the device and use it for traversing sewage. However, due to the system requiring a uniform magnetic field along its symmetry axis, the device can not be used for underground tube systems. As creating a uniform magnetic field from the outside of those underground tubes would require the tubes to be dug up. This would, however, not be the case for above-ground tube networks. The magnetic field could be created by two coils around the tube in question. These tube networks could be inspected from the inside out without interrupting the liquid flow.

10 Conclusion

In this thesis, an intravenous locomotion device has been designed. After setting up the requirements, 3 concepts were developed, from which the negative poisson ratio worm concept was chosen. This concept was adjusted to only consist of 3 modules. For each of these modules additional requirements were set up, with which the design was finalised. The modules were then tested separately to determine the expansion rate and folding behaviour of the modules. Then the modules were tested together inside an integration test. Against expectations, the integration test showed that the prototype moved forward, with as optimal input a square wave with a frequency of 2 HZ. Although this proves that this concept could work, there are still requirements not met with this prototype. The current prototype needs to decrease in size by 38 % and needs to be made out of fewer parts. It currently does not use biomaterials and can not move backwards. The system also needs to be tested in a better replica of the aorta to determine whether the design can navigate fluctuating diameters, does not damage the aortic wall and does not block blood flow too much. However, this thesis does provide a valid design for a magnetically actuated, origami-based locomotion device. Which with the given adjustments, could be able to navigate endovascular systems.

References

- [1] Collapsible Paper Tower Helix Decagon - YouTube. URL: <https://www.youtube.com/watch?v=sUyTAgTHmwE>.
- [2] Collapsible Tower Dodecagon V2 With Sectioned Folds - YouTube. URL: <https://www.youtube.com/watch?v=cG33Lvb2CfE>.
- [3] From Origami to Space Engineering: An Art Folding Every Limit - UX Connections. URL: <https://www.uxconnections.com/from-origami-to-space-engineering-an-art-folding-every-limit/>.
- [4] Help With 0.2 MM Nozzle - Improve your 3D prints - UltiMaker Community of 3D Printing Experts. URL: <https://community.ultimaker.com/topic/45581-help-with-02-mm-nozzle/>.
- [5] Houten bouwpakketten en modelbouw — Robotime Nederland. URL: <https://www.robotime.nl/collections/houten-bouwpakketten?page=1>.
- [6] How thin can a 3D printer print? — dddrop - Professional FFF 3D Printers - Additive manufacturing. URL: <https://dddrop.com/how-to-perfectly-print-a-thin-walled-3d-print/>.
- [7] How To Make an Origami Flapping Bird - EASY step by step! - YouTube. URL: <https://www.youtube.com/watch?v=DD1M3VrNSt4>.
- [8] Japanese Hobbies: CPs - The Crane. URL: <https://jaysjapanesehobbies.blogspot.com/2010/04/cps-crane.html>.
- [9] Origami - Japanese Art, Paper Folding, History — Britannica. URL: <https://www.britannica.com/art/origami/History-of-origami>.
- [10] Origami Simulator. URL: <https://origamisimulator.org/>.
- [11] Robotime Electric Guitar — Houten 3D DIY bouwset elektrische gitaar — Robotime Nederland. URL: <https://www.robotime.nl/products/robotime-electric-guitar>.
- [12] The Best Polyethylene & Polypropylene Glues — Bonding PP & PE Plastic. URL: <https://www.gluegun.com/blogs/news/best-adhesive-for-bonding-polypropylene-pp-and-polyethylene-pe>.
- [13] Tracker Video Analysis and Modeling Tool for Physics Education. URL: <https://physlets.org/tracker/>.
- [14] Why Polypropylene is so difficult to Bond ? - Adhesives & sealants engineering — Eng-Tips. URL: <https://www.eng-tips.com/threads/why-polypropylene-is-so-difficult-to-bond.78257/>.
- [15] Mohammad AL-Rawi, Ahmed M. AL-Jumaily, and Djelloul Belkacemi. Non-invasive diagnostics of blockage growth in the descending aorta-computational approach. *Medical & Biological Engineering & Computing*, 60(11):3265–3279, 11 2022. <https://doi.org/10.1007/s11517-022-02665-2> doi:10.1007/s11517-022-02665-2.
- [16] Allan John R. Barcena, Prashanth Ravi, Suprateek Kundu, and Karthik Tappa. Emerging Biomedical and Clinical Applications of 3D-Printed Poly(Lactic Acid)-Based Devices and Delivery Systems. *Bioengineering*, 11(7):705, 7 2024. URL: <https://pmc.ncbi.nlm.nih.gov/articles/PMC11273440/>, <https://doi.org/10.3390/BIOENGINEERING11070705> doi:10.3390/BIOENGINEERING11070705.
- [17] Besley Thomas. Bonding polypropylene with glue: Best methods and tips - ForgeWay Ltd. URL: <https://www.forgeWay.com/learning/blog/bonding-polypropylene-with-glue>.
- [18] Jared T. Bruton, Todd G. Nelson, Trent K. Zimmerman, Janette D. Fernelius, Spencer P. Magleby, and Larry L. Howell. Packing and deploying Soft Origami to and from cylindrical volumes with application to automotive airbags. *Royal Society Open Science*, 3(9), 9 2016. URL: <https://royalsocietypublishing.org/doi/10.1098/rsos.160429>, <https://doi.org/10.1098/RSOS.160429> doi:10.1098/RSOS.160429.

- [19] Ian Chaston. Technological Entrepreneurship: Technology-Driven vs Market-Driven Innovation. *Technological Entrepreneurship: Technology-Driven vs Market-Driven Innovation*, pages 1–299, 1 2017. <https://doi.org/10.1007/978-3-319-45850-2/COVER> doi:10.1007/978-3-319-45850-2/COVER.
- [20] Bogdan Ciszek, Krzysztof Cieřlicki, Paweł Krajewski, and Stefan K. Piechnik. Critical Pressure for Arterial Wall Rupture in Major Human Cerebral Arteries. *Stroke*, 44(11):3226–3228, 11 2013. <https://doi.org/10.1161/STROKEAHA.113.002370> doi:10.1161/STROKEAHA.113.002370.
- [21] Gastone Ciuti, R Calio, D Camboni, L Neri, F Bianchi, A Arezzo, A Koulaouzidis, S Schostek, D Stoyanov, C M Oddo, B Magnani, A Mencias, M Morino, M O Schurr, and P Dario. Frontiers of robotic endoscopic capsules: a review. *Journal of micro-bio robotics*, 11(1):1–18, 2016. URL: <https://pubmed.ncbi.nlm.nih.gov/29082124/http://www.pubmedcentral.nih.gov/articlerender.fcgi?artid=PMC5646258>, <https://doi.org/10.1007/S12213-016-0087-X> doi:10.1007/S12213-016-0087-X.
- [22] Margaret M Coad, Laura H Blumenschein, Sadie Cutler, Javier A Reyna Zepeda, Nicholas D Naclerio, Haitham El-Hussieny, Usman Mehmood, Jee-Hwan Ryu, Elliot W Hawkes, and Allison M Okamura. Vine Robots. *IEEE Robotics & Automation Magazine*, 27(3):120–132, 9 2020. <https://doi.org/10.1109/MRA.2019.2947538> doi:10.1109/MRA.2019.2947538.
- [23] Brian A Curran. Origami. *Encyclopaedia of the History of Science, Technology, and Medicine in Non-Western Cultures*, pages 1797–1800, 2008. URL: https://link.springer.com/referenceworkentry/10.1007/978-1-4020-4425-0_8818, https://doi.org/10.1007/978-1-4020-4425-0_8818 doi:10.1007/978-1-4020-4425-0_{_}8818.
- [24] Vincent DeStefano, Salaar Khan, and Alonzo Tabada. Applications of PLA in modern medicine. *Engineered Regeneration*, 1:76–87, 1 2020. <https://doi.org/10.1016/J.ENGREG.2020.08.002> doi:10.1016/J.ENGREG.2020.08.002.
- [25] David Dureisseix. An overview of mechanisms and patterns with origami. *International Journal of Space Structures*, 27(1):1–14, 3 2012. URL: https://www.researchgate.net/publication/257292764_An_Overview_of_Mechanisms_and_Patterns_with_Origami, <https://doi.org/10.1260/0266-3511.27.1.1> doi:10.1260/0266-3511.27.1.1.
- [26] Yomna Elghazi, Ayman Wagdy, Sahar Abdelwahab, and Asmaa Hassan. Daylighting Driven Design: Optimizing Kaleidocycle façade for hot arid climate. 11 2014. <https://doi.org/10.13140/RG.2.1.3198.4408> doi:10.13140/RG.2.1.3198.4408.
- [27] Hongbin Fang, Yetong Zhang, and K W Wang. Origami-based earthworm-like locomotion robots. *Bioinspiration & Biomimetics*, 12(6):065003, 10 2017. URL: <https://iopscience.iop.org/article/10.1088/1748-3190/aa8448>, <https://doi.org/10.1088/1748-3190/aa8448> doi:10.1088/1748-3190/aa8448.
- [28] J. M. Fitzpatrick and J. E.A. Wickham. Minimally invasive surgery. *The British journal of surgery*, 77(7):721–722, 1990. URL: <https://pubmed.ncbi.nlm.nih.gov/2200553/>, <https://doi.org/10.1002/BJS.1800770702> doi:10.1002/BJS.1800770702.
- [29] William E. Frazier. Metal additive manufacturing: A review. *Journal of Materials Engineering and Performance*, 23(6):1917–1928, 4 2014. URL: <https://link.springer.com/article/10.1007/s11665-014-0958-z>, <https://doi.org/10.1007/S11665-014-0958-Z/FIGURES/9> doi:10.1007/S11665-014-0958-Z/FIGURES/9.
- [30] Yukun Ge, Thilina Dulantha Lalitharatne, and Thrishantha Nanayakkara. Origami Inspired Design for Capsule Endoscope to Retrograde Using Intestinal Peristalsis. *IEEE Robotics and Automation Letters*, 7(2):5429–5435, 4 2022. <https://doi.org/10.1109/LRA.2022.3157406> doi:10.1109/LRA.2022.3157406.
- [31] Ian Gibson, David Rosen, Brent Stucker, and Mahyar Khorasani. *Additive Manufacturing Technologies*. 2021.



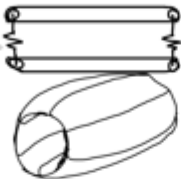

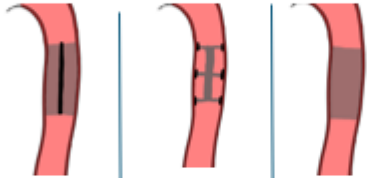

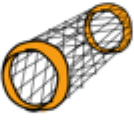
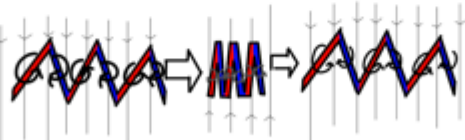
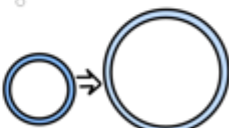

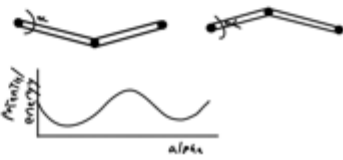
- [32] Jonathan Golledge. Abdominal aortic aneurysm: update on pathogenesis and medical treatments. *Nature Reviews Cardiology* 2018 16:4, 16(4):225–242, 11 2018. URL: <https://www.nature.com/articles/s41569-018-0114-9>, <https://doi.org/10.1038/s41569-018-0114-9> doi:10.1038/s41569-018-0114-9.
- [33] Satyabodh Shesharaj Guttal, Ramesh K. Nadiger, and Pravinkumar Shetty. Cytotoxic effect of indigenously fabricated dental magnets for application in prosthodontics. *Journal of Indian Prosthodontist Society*, 18(1):29–34, 1 2018. URL: https://journals.lww.com/jips/fulltext/2018/18010/cytotoxic_effect_of_indigenously_fabricated_dental.6.aspx, <https://doi.org/10.4103/JIPS.JIPS.114.17> doi:10.4103/JIPS.JIPS{_}_114{_}_17.
- [34] Solomon Russom Habtay. A Firm-Level Analysis on the Relative Difference between Technology-Driven and Market-Driven Disruptive Business Model Innovations. *Creativity and Innovation Management*, 21(3):290–303, 9 2012. <https://doi.org/10.1111/J.1467-8691.2012.00628.X> doi:10.1111/J.1467-8691.2012.00628.X.
- [35] <https://flowtoys.com/toroflux?srsltid=AfmBOopNcKq84draGfCjx5LjtTqwWbr-NU5NsemcauNxcQ1ba-FEYz6o> and 28-11-2024. Toroflux.
- [36] Jian Huang, Yongsheng Wang, Lin Lin, Zhibin Li, Zhonggui Shan, and Shaoyi Zheng. Comparison of dynamic changes in aortic diameter during the cardiac cycle measured by computed tomography angiography and transthoracic echocardiography. *Journal of Vascular Surgery*, 69(5):1538–1544, 5 2019. <https://doi.org/10.1016/j.jvs.2018.07.083> doi:10.1016/j.jvs.2018.07.083.
- [37] B. Jaffray. Minimally invasive surgery. *Archives of disease in childhood*, 90(5):537–542, 5 2005. URL: <https://pubmed.ncbi.nlm.nih.gov/15851444/>, <https://doi.org/10.1136/ADC.2004.062760> doi:10.1136/ADC.2004.062760.
- [38] Jaisohn Kim VT. Coding the Mass-Spring-Damper System in MATLAB (2/2).
- [39] Semi Jeong, Hyunchul Choi, Gwangjun Go, Cheong Lee, Kyung Seob Lim, Doo Sun Sim, Myung Ho Jeong, Seong Young Ko, Jong Oh Park, and Sukho Park. Penetration of an artificial arterial thromboembolism in a live animal using an intravascular therapeutic microrobot system. *Medical Engineering & Physics*, 38(4):403–410, 4 2016. <https://doi.org/10.1016/J.MEDENGPY.2016.01.001> doi:10.1016/J.MEDENGPY.2016.01.001.
- [40] K.Wayne Johnston, Robert B. Rutherford, M.David Tilson, Dhiraj M. Shah, Larry Hollier, and James C. Stanley. Suggested standards for reporting on arterial aneurysms. *Journal of Vascular Surgery*, 13(3):452–458, 3 1991. <https://doi.org/10.1067/mva.1991.26737> doi:10.1067/mva.1991.26737.
- [41] Corinne Kruger and Nigel Cross. Solution driven versus problem driven design: strategies and outcomes. *Design Studies*, 27(5):527–548, 9 2006. <https://doi.org/10.1016/J.DESTUD.2006.01.001> doi:10.1016/J.DESTUD.2006.01.001.
- [42] Mohit Kshirsagar, Siddhi D. Ambike, Niranjana Jaya Prakash, Balasubramanian Kandasubramanian, and Pradnya Deshpande. Origami engineering: Creating dynamic functional materials through folded structures. *Hybrid Advances*, 4:100092, 12 2023. <https://doi.org/10.1016/J.HYBADV.2023.100092> doi:10.1016/J.HYBADV.2023.100092.
- [43] Robert J. Lang, Nathan Brown, Brian Ignaut, Spencer Magleby, and Larry Howell. Rigidly Foldable Thick Origami Using Designed-Offset Linkages. *Journal of Mechanisms and Robotics*, 12(2), 4 2020. <https://doi.org/10.1115/1.4045940> doi:10.1115/1.4045940.
- [44] Ruihua Li, Yang Liu, and Jianjun Jiang. Research advances in drug therapy for abdominal aortic aneurysms over the past five years: An updated narrative review. *International Journal of Cardiology*, 372:93–100, 2 2023. <https://doi.org/10.1016/J.IJCARD.2022.11.058> doi:10.1016/J.IJCARD.2022.11.058.

- [45] Patrick Z. McVeigh, Raphael Sacho, Robert A. Weersink, Vitor M. Pereira, Walter Kucharczyk, Eric J. Seibel, Brian C. Wilson, and Timo Krings. High-Resolution Angioscopic Imaging During Endovascular Neurosurgery. *Neurosurgery*, 75(2):171, 2014. URL: <https://pmc.ncbi.nlm.nih.gov/articles/PMC4086773/>, <https://doi.org/10.1227/NEU.0000000000000383> doi:10.1227/NEU.0000000000000383.
- [46] Shuhei Miyashita, Steven Guitron, Kazuhiro Yoshida, Shuguang Li, Dana D. Damian, and Daniela Rus. Ingestible, controllable, and degradable origami robot for patching stomach wounds. In *2016 IEEE International Conference on Robotics and Automation (ICRA)*, pages 909–916. IEEE, 5 2016. <https://doi.org/10.1109/ICRA.2016.7487222> doi:10.1109/ICRA.2016.7487222.
- [47] Elissa Morris, Daniel A. McAdams, and Richard Malak. The State of the Art of Origami-Inspired Products: A Review. *Proceedings of the ASME Design Engineering Technical Conference*, 5B-2016, 12 2016. URL: <https://dx.doi.org/10.1115/DETC2016-59629>, <https://doi.org/10.1115/DETC2016-59629> doi:10.1115/DETC2016-59629.
- [48] Kirsty Muldoon, Yanhua Song, Zeeshan Ahmad, Xing Chen, and Ming Wei Chang. High Precision 3D Printing for Micro to Nano Scale Biomedical and Electronic Devices. *Micromachines* 2022, Vol. 13, Page 642, 13(4):642, 4 2022. URL: <https://www.mdpi.com/2072-666X/13/4/642/html><https://www.mdpi.com/2072-666X/13/4/642>, <https://doi.org/10.3390/MI13040642> doi:10.3390/MI13040642.
- [49] Ian M. Nordon, Robert J. Hinchliffe, Ian M. Loftus, and Matt M. Thompson. Pathophysiology and epidemiology of abdominal aortic aneurysms. *Nature Reviews Cardiology*, 8(2):92–102, 2 2011. <https://doi.org/10.1038/nrcardio.2010.180> doi:10.1038/nrcardio.2010.180.
- [50] Rui Peng and Gregory S. Chirikjian. A methodology for thick-panel origami pattern design. *Mechanism and Machine Theory*, 189:105423, 11 2023. <https://doi.org/10.1016/j.mechmachtheory.2023.105423> doi:10.1016/j.mechmachtheory.2023.105423.
- [51] Rui Peng and Gregory S. Chirikjian. Morphable thick-panel origami. *Mechanism and Machine Theory*, 192:105528, 2 2024. <https://doi.org/10.1016/j.mechmachtheory.2023.105528> doi:10.1016/j.mechmachtheory.2023.105528.
- [52] Nelson G Badillo Perez and Margaret M Coad. Self-Propelled Soft Everting Toroidal Robot for Navigation and Climbing in Confined Spaces. In *2022 IEEE/RSJ International Conference on Intelligent Robots and Systems (IROS)*, pages 5409–5415, 10 2022. <https://doi.org/10.1109/IROS47612.2022.9981175> doi:10.1109/IROS47612.2022.9981175.
- [53] Hossein Ramezani Ali-Akbari. Design-of-a-Satellite-Solar-Panel-Deployment-Mechanism-Using-the-Brushed-DC-Motor-as-Rotational-Speed-Damper. 1 2018.
- [54] Gulnaaz Rasiya, Abhinav Shukla, and Karan Saran. Additive Manufacturing-A Review. *Materials Today: Proceedings*, 47:6896–6901, 1 2021. <https://doi.org/10.1016/J.MATPR.2021.05.181> doi:10.1016/J.MATPR.2021.05.181.
- [55] Kenny Seymour, Dakota Burrow, Alex Avila, Terri Bateman, David Morgan, Spencer Magleby, and Larry Howell. Origami-Based Deployable Ballistic Barrier. *Faculty Publications*, 9 2018. URL: <https://scholarsarchive.byu.edu/facpub/2981>.
- [56] Metin Sitti, Hakan Ceylan, Wenqi Hu, Joshua Giltinan, Mehmet Turan, Sehyuk Yim, and Eric Diller. Biomedical Applications of Untethered Mobile Milli/Microrobots. *Proceedings of the IEEE*, 103(2):205–224, 2 2015. <https://doi.org/10.1109/JPROC.2014.2385105> doi:10.1109/JPROC.2014.2385105.
- [57] P.W. Stather, D.A. Sidloff, I.A. Rhema, E. Choke, M.J. Bown, and R.D. Sayers. A Review of Current Reporting of Abdominal Aortic Aneurysm Mortality and Prevalence in the Literature. *European Journal of Vascular and Endovascular Surgery*, 47(3):240–242, 3 2014. <https://doi.org/10.1016/j.ejvs.2013.11.007> doi:10.1016/j.ejvs.2013.11.007.
- [58] Stephan Haulon. Golden rules to perform complex EVAR in daily practice, 5 2017. URL: <https://www.youtube.com/watch?v=f3yAbWPnZq>.

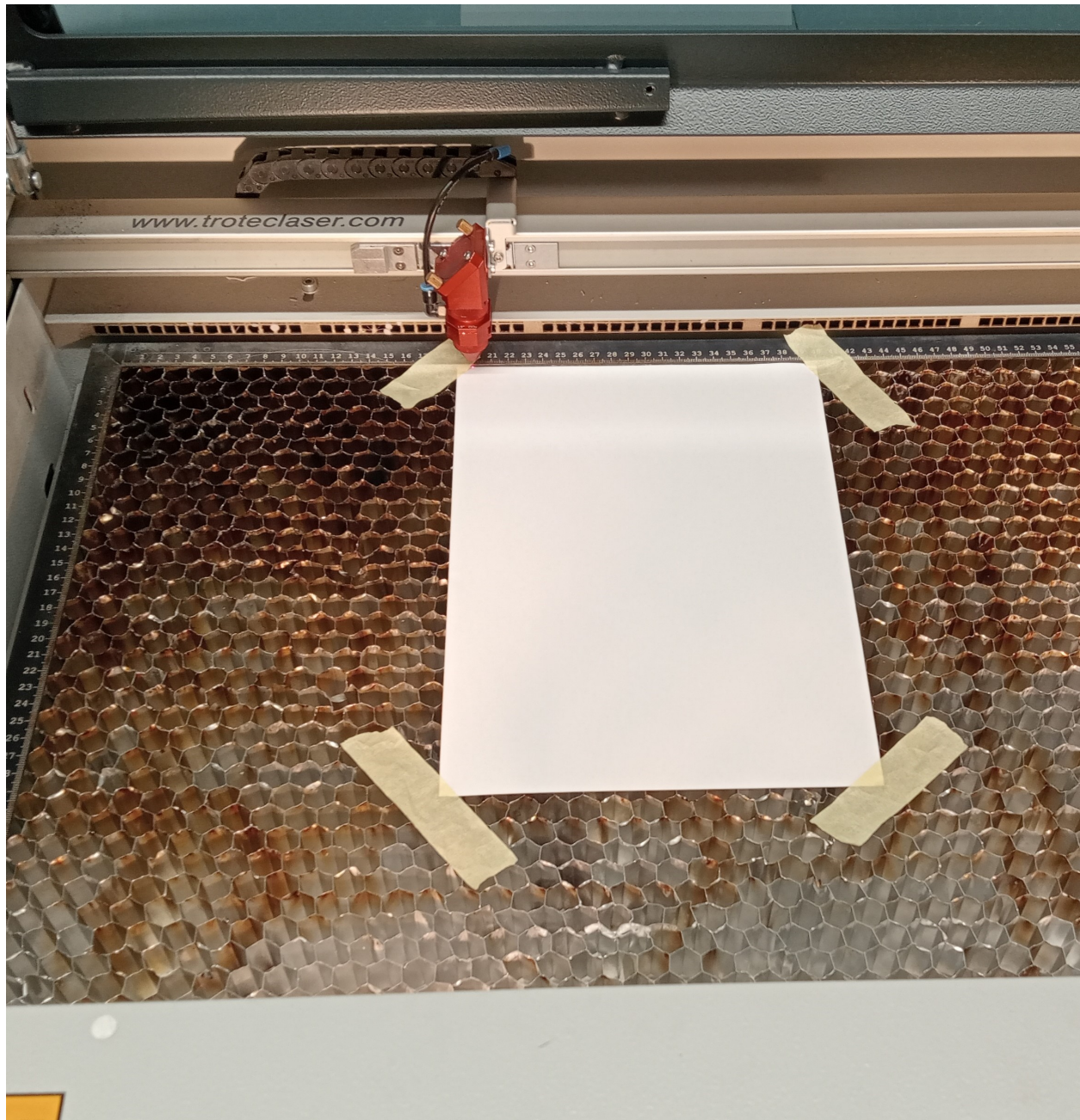
- [59] Austin Taylor, Matthew Miller, Mable Fok, Kent Nilsson, and Zion Tsz Ho Tse. Intracardiac magnetic resonance imaging catheter with origami deployable mechanisms. *Journal of Medical Devices, Transactions of the ASME*, 10(2), 6 2016. URL: <https://dx.doi.org/10.1115/1.4033151>, <https://doi.org/10.1115/1.4033151/377278> doi:10.1115/1.4033151/377278.
- [60] Sam Tijhuis. *A Modeling Framework for Magnetic Origami Devices using a Bar-and-Hinge Model*. PhD thesis, 6 2024.
- [61] G M Van Vliet. *DESIGN OF A COMPLIANT MAGNETIC CAPSULE ROBOT FOR UNTETHERED CARDIOVASCULAR SURGICAL TOOLS*. PhD thesis, 2021.
- [62] Kaufui V. Wong and Aldo Hernandez. A Review of Additive Manufacturing. *International Scholarly Research Notices*, 2012(1):208760, 1 2012. URL: <https://onlinelibrary.wiley.com/doi/full/10.5402/2012/208760><https://onlinelibrary.wiley.com/doi/abs/10.5402/2012/208760><https://onlinelibrary.wiley.com/doi/10.5402/2012/208760>, <https://doi.org/10.5402/2012/208760> doi:10.5402/2012/208760.
- [63] Oncay Yasa, Yasunori Toshimitsu, Mike Y. Michelis, Lewis S. Jones, Miriam Filippi, Thomas Buchner, and Robert K. Katzschmann. An Overview of Soft Robotics. *Annual Review of Control, Robotics, and Autonomous Systems*, 6(Volume 6, 2023):1–29, 5 2023. URL: <https://www.annualreviews.org/content/journals/10.1146/annurev-control-062322-100607>, <https://doi.org/10.1146/ANNUREV-CONTROL-062322-100607/CITE/REFWORKS> doi:10.1146/ANNUREV-CONTROL-062322-100607/CITE/REFWORKS.
- [64] Hiromi Yasuda, Yasuhiro Miyazawa, Efstathios G. Charalampidis, Christopher Chong, Panayotis G. Kevrekidis, and Jinkyu Yang. Origami-based impact mitigation via rarefaction solitary wave creation. *Science Advances*, 5(5), 2019. URL: <https://www.science.org/doi/10.1126/sciadv.aau2835>, https://doi.org/10.1126/SCIADV.AAU2835/SUPPL_FILE/AAU2835.SM.PDF doi:10.1126/SCIADV.AAU2835/SUPPL{_}FILE/AAU2835{_}SM.PDF.
- [65] Sishen Yuan, Sifan Cao, Junnan Xue, Shijian Su, Junyan Yan, Min Wang, Wenchao Yue, Shing Shin Cheng, Jun Liu, Jiaole Wang, Shuang Song, Max Q.H. Meng, and Hongliang Ren. Versatile Motion Generation of Magnetic Origami Spring Robots in the Uniform Magnetic Field. *IEEE Robotics and Automation Letters*, 7(4):10486–10493, 10 2022. <https://doi.org/10.1109/LRA.2022.3194318> doi:10.1109/LRA.2022.3194318.
- [66] Abolfazl Zolfaghari, Tiantong Chen, and Allen Y. Yi. Additive manufacturing of precision optics at micro and nanoscale. *International Journal of Extreme Manufacturing*, 1(1):012005, 4 2019. URL: <https://iopscience.iop.org/article/10.1088/2631-7990/ab0fa5><https://iopscience.iop.org/article/10.1088/2631-7990/ab0fa5/meta>, <https://doi.org/10.1088/2631-7990/AB0FA5> doi:10.1088/2631-7990/AB0FA5.

11 Appendix

11.1 Morphological diagram

Key features	Options	
Locomotion		
		
Aortic adaptability		
Base shape		
Modulation method		
		

11.2 Lasercutter setup



11.3 Lasercutter results

11.3.1 Results 50g paper

p	12	9	6	4,5	3	p	12	9	6	4,5	3
g	2,5	2,5	2,5	2,5	2,5	g	4	4	4	4	4

12	9	6	4,5	3	12	9	6	4,5	3
5	5	5	5	5	2,5	2,5	2,5	2,5	2,5

12	9	6	4,5	3	12	9	6	4,5	3
10	10	10	10	10	10	10	10	10	10

11.3.2 Results 80g paper

12	9	6	4,5	3
2,5	2,5	2,5	2,5	2,5

12	9	6	4,5	3
4	4	4	4	4

12	9	6	4,5	3
5	5	5	5	5

12	9	6	4,5	3
7,5	7,5	7,5	7,5	7,5

12	9	6	4,5	3
10	10	10	10	10

11.3.3 Result table

Table 11: Results 50 gsm paper. C=cut, C/G=Almost good engraving but parts are cut, G=good engraving, G/N=There is engraving but it is very shallow, N=no engraving, P=perforation

power%\speed	2.5	4	5	7.5	10
3	G/N	N	N	N	N
4.5	C/G	G	N	N	N
6	C	C/G	G	G/N	N
9	C	C	C/G	G	P
12	C	C	C	C/G	P

Table 12: Results 80 gsm paper. C=cut, C/G=Almost good engraving but parts are cut, G=good engraving, G/N=There is engraving but it is very shallow, N=no engraving, P=perforation

power%\speed	2.5	4	5	7.5	10
3	G/N	N	N	N	N
4.5	C/G	G/N	N	N	N
6	C	G	G	N	N
9	C	C/G	P	P	P
12	C	C	C	G	G

11.4 Mass-spring-damper model

11.4.1 background

11.5 Mass-spring-damper model

To model the behaviour of the modules a Mass-Spring-Damper (MSD) model is used. As the name suggests an MSD model consists of a virtual mass connected to the ground via a spring and a damper. The mass in the model used in this thesis has 1 Degree Of Freedom (DOF), meaning that the mass can only move up and down; this displacement will be called x . The last part of the MSD model is an external force, F , acting on the mass. This model is visualised in Fig 44.

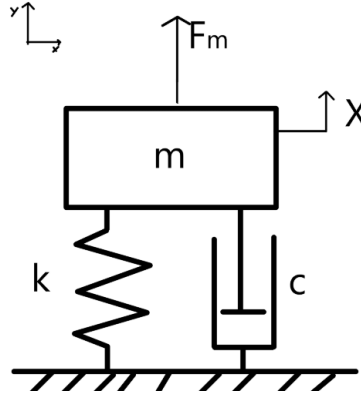


Figure 44: Sketch of a 1 DOF MSD Model

The spring with stiffness k pushes and pulls the mass towards a desired point. However, without a damper, the mass will always be oscillating. This is similar to a pendulum swing trying to get the ball to the lowest point but constantly overshooting, resulting in the oscillating behaviour the swing is known for. The damper takes energy out of the system and slows down the mass, stopping the oscillation of the mass. For the pendulum swing example, the damper is air, reducing the speed of the swing and taking energy out of the system and converting it into the air, eventually resulting in the swing hanging statically at the bottom of the rope.

Using the equation of motion of the MSD model predictions can be made on the behaviour of the system. This can be done by analysing the damping ratio, this ratio is calculated as follows:

$$F_m - kx - c\dot{x} = m\ddot{x} \quad (3)$$

$$\zeta = \frac{c}{2m\omega_n} \quad \text{where} \quad \omega_n = \frac{k}{m} \quad (4)$$

The system can be undamped ($\zeta = 0$), underdamped ($\zeta < 1$), critically damped ($\zeta = 1$), or overdamped ($\zeta > 1$). To calculate the movement of the model a Matlab script made by Jaison Kim VT was used as the basis and modified to fit the desired model [38].

11.5.1 MSD

To improve the parameters of the prototype a model needs to be made to simulate the behaviour of the entire modules inside a magnetic field. Previously in this thesis, a model made by Sam Tijhuis was used to simulate the behaviour of the modules. This model can not be reused for two reasons. The first reason is that this model focuses on individual tiles in small scale, full 4x8 tessellations patterns are not possible, thus the assumption must be made that all tiles behave the same and do not significantly interact with each other. But even if a strong enough computer can be found The second reason is that both RM and collapsable tower need to be folded from a tube of paper, not a flat piece of paper. This adjustment is not possible

in the Sam's current model. The solution to both problems is to either, upgrade the model to use more tessellations and give the program the ability to fold paper tubes instead of flat pieces of paper or develop a new model focussing on the behaviour of the module in its entirety. During the production of the prototypes of the modules, it was noticed how the module behaved similarly to a Mass-spring-damper model, thus in this chapter a model of the module expansion rate based on the MSD model is proposed.

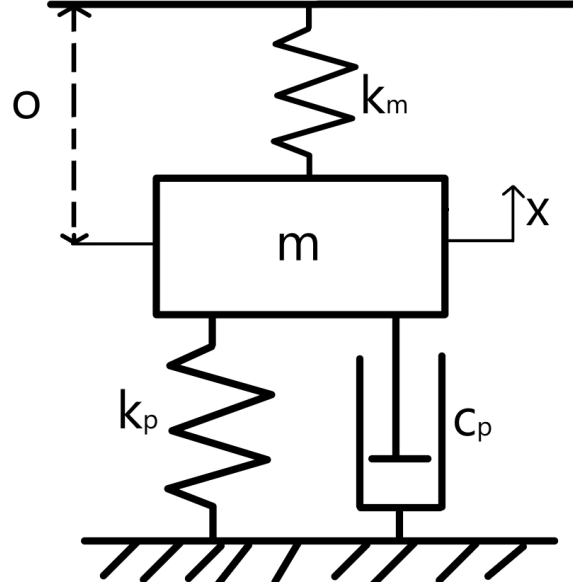


Figure 45: Altered MSD model used in this thesis for simulating the individual behaviour of the modules

11.5.2 Creating the model

To start, a module (does not matter which) is seen as a black box. The input of this box is the force created by the magnets inside the magnetic field, the output would be the expansion of the module. A model to fit the black box would be the 1 Degree of Freedom (DOF) Mass-Spring-Damper Model (MSDM). Force F can be defined as being linearly proportional to the torque created by the magnets inside the magnetic field, so $\tau = F_m * n$ where τ is the torque created by the magnets, F_m is the force inside the model and n is a constant. Following that, to fully fit the model inside the black box, the assumption is made that the displacement x is linearly proportional to the expansion percentage of the module, so $x = \text{expansion percentage} * n$ where n is once again a constant. A visualisation of this model can be seen in Fig 45

Now that this model fits the black box, the equation of motion can be derived

$$\sum F = ma \quad (5)$$

$$\sum F = m\ddot{x} \quad (6)$$

Then insert the force created by the spring and the damper and the external force F_m .

$$F_m - kx - c\dot{x} = m\ddot{x} \quad (7)$$

Now before doing any calculations, F_m needs to be addressed. This force is not constant as in chapter 11.5. But should be seen as a non-linear spring. The torque created by the magnets can be calculated using $\tau = M \times B$. As the error between the magnets and magnetic field direction decreases the torque created decreases as well, along a sinus curve. The reason that the torque is proportional to the error along a sinuswave is because the cross product formula can also be written as

$$\tau = |M||B|\sin(\theta) \quad (8)$$

Where theta is the difference in angle between the dipole magnets and the magnetic field. So inserting $F_m = \tau$ to this formula creates $F_m = |M||B|\sin(\theta)n$. Knowing that $F_m = 0$ during a total collapse and when the module is totally open, means that when x is equal to the geometric maximum expansion percentage or equal to the geometric minimum expansion percentage than F_m is 0. Assuming $x=0$ lies in the middle, then $\sin(\theta)$ can be rewritten as $\cos(\pi\frac{x}{o})$. That only leaves the parameters $|M|$, $|B|$, and n . These variables Magnetic dipole, field strength, and constant n are all constant in our simulation and are summarised as value k_m . This resulted in the following equations of motion.

$$F_m - kx - c\dot{x} = m\ddot{x} \quad (9)$$

$$m\ddot{x} + k_px + c_p\dot{x} - k_m(\cos(\pi\frac{x}{o})) = 0 \quad (10)$$

The translation from model parameter to real life parameter is summarised in Table 13 and is as follows: Reducing mass in the model (m) is the same as reducing mass and or inertia in the module. Reducing the k_p is making the creases of the paper less stiff. Reducing damping reduces the main losses of energy in the system: friction, and material deformation. Increasing k_m increases the magnetic field, the number of magnets in the module or, the strength of the magnets.

Table 13: Parameters used in the MSD model and its real life counterparts

Model	Real module
x	Current expansion percentage
o	Geometric maximum expansion percentage
m	Inertia and Mass
k_p	Stiffness of the creases
k_m	Coefficient for magnetic power (nr of magnets, magnetic field strength)
C_p	Coefficient for energy loss (friction, deformation)

11.5.3 Finding the correct parameters

Now that a model has been created the correct parameter values need to be found. This was done by making the model simulate the experiment of the quickly changing field found in chapter 6.3. A blind guess was made for the parameters and the resulting behaviour was compared to the results from the real-life experiment. Then adjustments were made to the parameters and the behaviour was compared again. This continued until the behaviour was close enough to reality. The result of the final configuration compared to reality can be found in Fig 46. The parameters used in this configuration can be found in table 14.

Table 14: Parameter values used in simulation

Variable	RM expanding	RM decreasing	AXM expanding	AXM decreasing
o	250	TBD	TBD	TBD
m	0.01	TBD	TBD	TBD
k_p	3.75	TBD	TBD	TBD
k_m	26.25	TBD	TBD	TBD
c_p	0.19	TBD	TBD	TBD

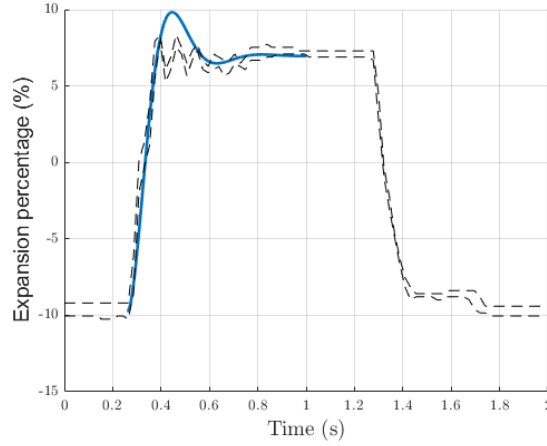


Figure 46: Graph visualising difference between model and reality. Blue: Simulation. Black-dashed: Max and Min values of prototype during experiment.

11.5.4 Using the model to find prototype improvements

Now that the model has the correct parameters to simulate the prototype, the parameters can be adjusted to see the impact

RM expansionrate The expansion rate of the simulation is fully determined by the ratio between k_p and k_m . Increasing k_m while reducing k_p increases the expansionrate. In cases where k_m and k_p are close in value, the expansionrate can be approximated with the following formula $\text{expansionrate} = 2 \frac{k_m+1}{k_p}$. This formula stops being effective once k_m becomes much larger than k_p . As at a factor of 25 the simulated expansion rate is 46.0%, two entire percentage of the expected 48%. At a factor of 50 the expansionrate is 84% an entire 16% lower than expected. This reduction is because as x increase k_m reduces in effectivity while k_p is modeled as a linear spring and behaves similar at all expansion percentages.

The expansion rate requirement was set at 19%, this means an expansion from zero of $\pm 8.5\%$. To achieve this expansion percentage the ratio between k_m and k_p needs to be at least 8.5 to 1. The ratio of the current prototype is 7 to 1, see Fig ???. So to fulfill the requirement of 19% expansion either the paper needs to reduce its stiffness with a factor of 1.19, or the magnetic interaction needs to increase by a factor of 1.19. Either by adding stronger magnets or increasing the field to 60mT. Although the field can not increase its magnetic field, reducing the crease stiffness or increasing the magnetic strength by a factor of 1.19 should be possible.

That all being said, the expansion target in the requirements was set at 100%, the correct ratio for this expansionrate of k_m and k_p was found to be 64 to 1. This leads to an expansionrate of 100.0%, as can be seen in Fig ??. This means that in order for the prototype to reach at least an expansion rate of 100% either the crease stiffness needs to decrease by a factor of 9.2. Or the magnetic interaction needs to increase by a factor of 9.2. As placing 10 times more magnets, or increasing the magnetic field to 460mT is not possible, the best plan of action would be to reduce the stiffness of the creases. Perforating the paper more often or using a material 9.2 times less stiff than paper are two potential solutions that could lead to the desired expansionrate of 100%.

AXM speed *Needs to be written

11.5.5 Shortcomings of the model

The MDSM model is not flawless relative to the model by Sam. In the MDS model certain individual real life parameters are more difficult to link to virtual ones. For example when a paper joint is folded with more force the zero point of the zero point of the spring is set to a different angle. This is a simple adjustment in Sam's model. In the MDSM various variables all need to be adjusted x_e , k_m , and k_p to change this one parameter.

11.5.6 Conclusion

Although this model is not perfect it provides insight in the effects of changing certain parameters of both the RM as the AXM. The resting expansion value is proportional to the k_m/k_p . Decreasing k_p of the current RM prototype by a factor of 50 is needed in order for the RM to fulfill its goal expansion of 100%. The reaction speed of the system is controlled by all factors. A reduction in mass, k_p , and damping reduces the reaction speed. The same effect happens when increasing k_m or γ . The best method to reduce the speed of the AXM is by xxx.

11.6 Results integration experiment

